Space Research Institute Graz
Austrian Academy of Sciences

Specific aspects of magnetospheric physics

Non-thermal radio emissions
In-situ and remote sensing

Helmut O. Rucker

CERN, Geneve, June 2006

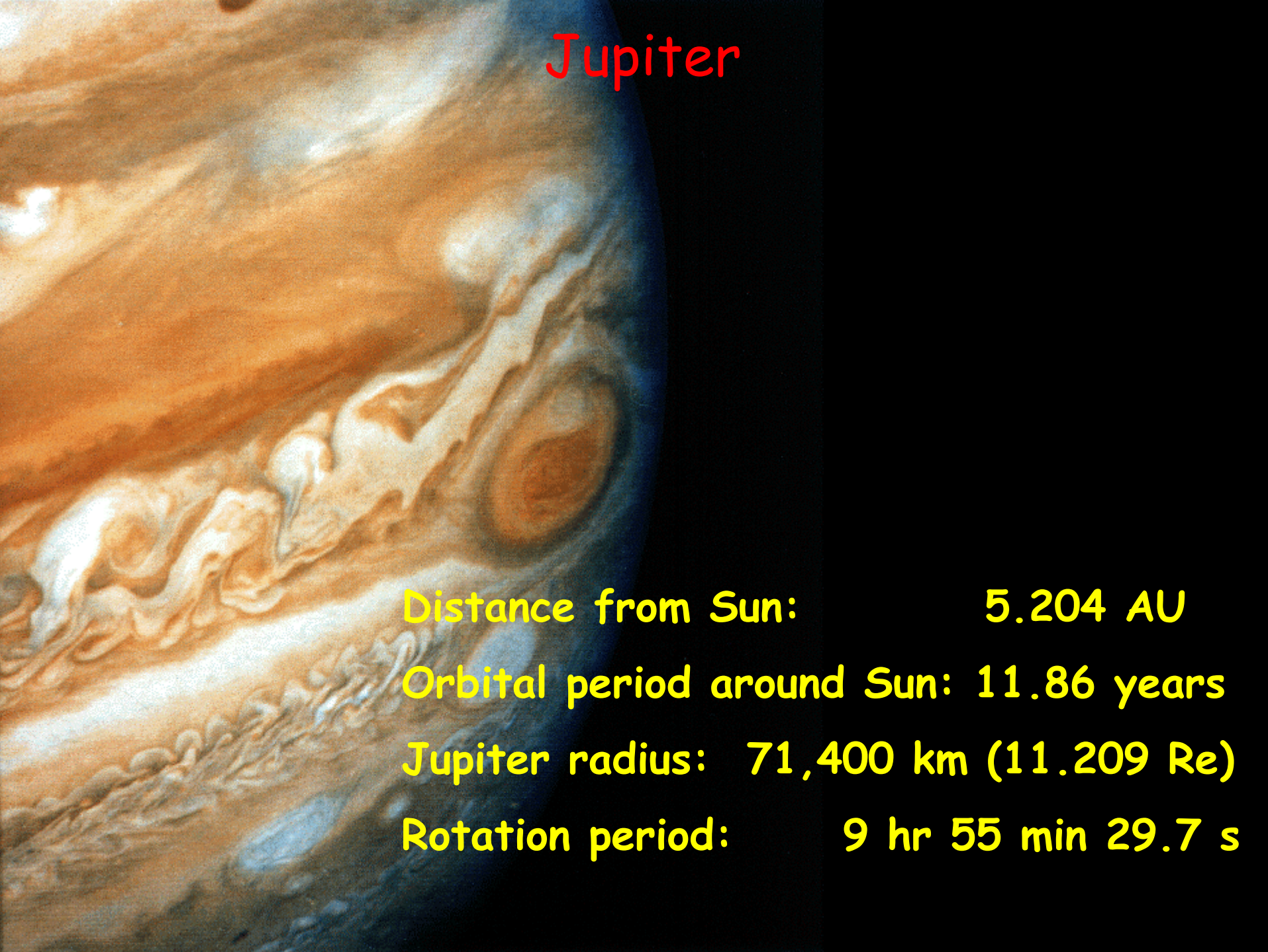
Jupiter
Distance from Sun: 5.204 AU
Orbital period around Sun: 11.86 years
Jupiter radius: 71,400 km (11.209 Re)
Rotation period: 9 hr 55 min 29.7 s

6th International Workshop on „Planetary Radio Emissions“ (PRE VI)

Bernhard F. Burke (MIT, USA):

Planetary Radio Astronomy: Fifty Years Ago and Fifty Years Hence

April 20 – 22, 2005

Graz, Austria

The early days of Planetary Radio Astronomy

JOURNAL OF GEOPHYSICAL RESEARCH VOLUME 60, No. 2 JUNE, 1955

OBSERVATIONS OF A VARIABLE RADIO SOURCE ASSOCIATED WITH THE PLANET JUPITER

BY B. F. BURKE AND K. L. FRANKLIN

Department of Terrestrial Magnetism, Carnegie Institution of Washington, Washington 15, D. C.

(Received April 15, 1955)

ABSTRACT

A source of variable 22.2-Mc/sec radiation has been detected with the large "Mills Cross" antenna of the Carnegie Institution of Washington. The source is present on nine records out of a possible 31 obtained during the first quarter of 1955. The appearance of the records of this source resembles that of terrestrial interference, but it lasts no longer than the time necessary for a celestial object to pass through the antenna pattern. The derived position in the sky corresponds to the position of Jupiter and exhibits the geocentric motion of Jupiter. There is no evident correlation between the times of appearance of this phenomenon and the rotational period of the planet Jupiter, or with the occurrence of solar activity. There is evidence that most of the radio energy is concentrated at frequencies lower than 38 Mc/sec.

The early days of Planetary Radio Astronomy

JOURNAL OF GEOPHYSICAL RESEARCH VOLUME 60, No. 2 JUNE, 1955

OBSERVATIONS OF A VARIABLE RADIO SOURCE ASSOCIATED WITH THE PLANET JUPITER

BY B. F. BURKE AND K. L. FRANKLIN

Department of Terrestrial Magnetism, Carnegie Institution of Washington, Washington 15, D. C.

(Received April 15, 1955)

ABSTRACT

A source of variable 22.2-Mc/sec radiation has been detected with the large "Mills Cross" antenna of the Carnegie Institution of Washington. The source is present on nine records out of a possible 31 obtained during the first quarter of 1955. The appearance of the records of this source resembles that of terrestrial interference, but it lasts no longer than the time necessary for a celestial object to pass through the antenna pattern. The derived position in the sky corresponds to the position of Jupiter and exhibits the geocentric motion of Jupiter. There is no evident correlation between the times of appearance of this phenomenon and the rotational period of the planet Jupiter, or with the occurrence of solar activity. There is evidence that most of the radio energy is concentrated at frequencies lower than 38 Mc/sec.

Bernie Burke
in PRE VI Proceedings 2006:

„Finding that Jupiter was a powerful source of radio noise was completely unexpected fifty years ago.

The early days of Planetary Radio Astronomy

JOURNAL OF GEOPHYSICAL RESEARCH VOLUME 60, No. 2 JUNE, 1955

OBSERVATIONS OF A VARIABLE RADIO SOURCE ASSOCIATED WITH THE PLANET JUPITER

BY B. F. BURKE AND K. L. FRANKLIN

Department of Terrestrial Magnetism, Carnegie Institution of Washington, Washington 15, D. C.

(Received April 15, 1955)

ABSTRACT

A source of variable 22.2-Mc/sec radiation has been detected with the large "Mills Cross" antenna of the Carnegie Institution of Washington. The source is present on nine records out of a possible 31 obtained during the first quarter of 1955. The appearance of the records of this source resembles that of terrestrial interference, but it lasts no longer than the time necessary for a celestial object to pass through the antenna pattern. The derived position in the sky corresponds to the position of Jupiter and exhibits the geocentric motion of Jupiter. There is no evident correlation between the times of appearance of this phenomenon and the rotational period of the planet Jupiter, or with the occurrence of solar activity. There is evidence that most of the radio energy is concentrated at frequencies lower than 38 Mc/sec.

Bernie Burke
in PRE VI Proceedings 2005:

„Finding that Jupiter was a powerful source of radio noise was completely unexpected fifty years ago.

The textbooks had nothing to say about what the radio properties of the planets might be …“

The early days of Planetary Radio Astronomy

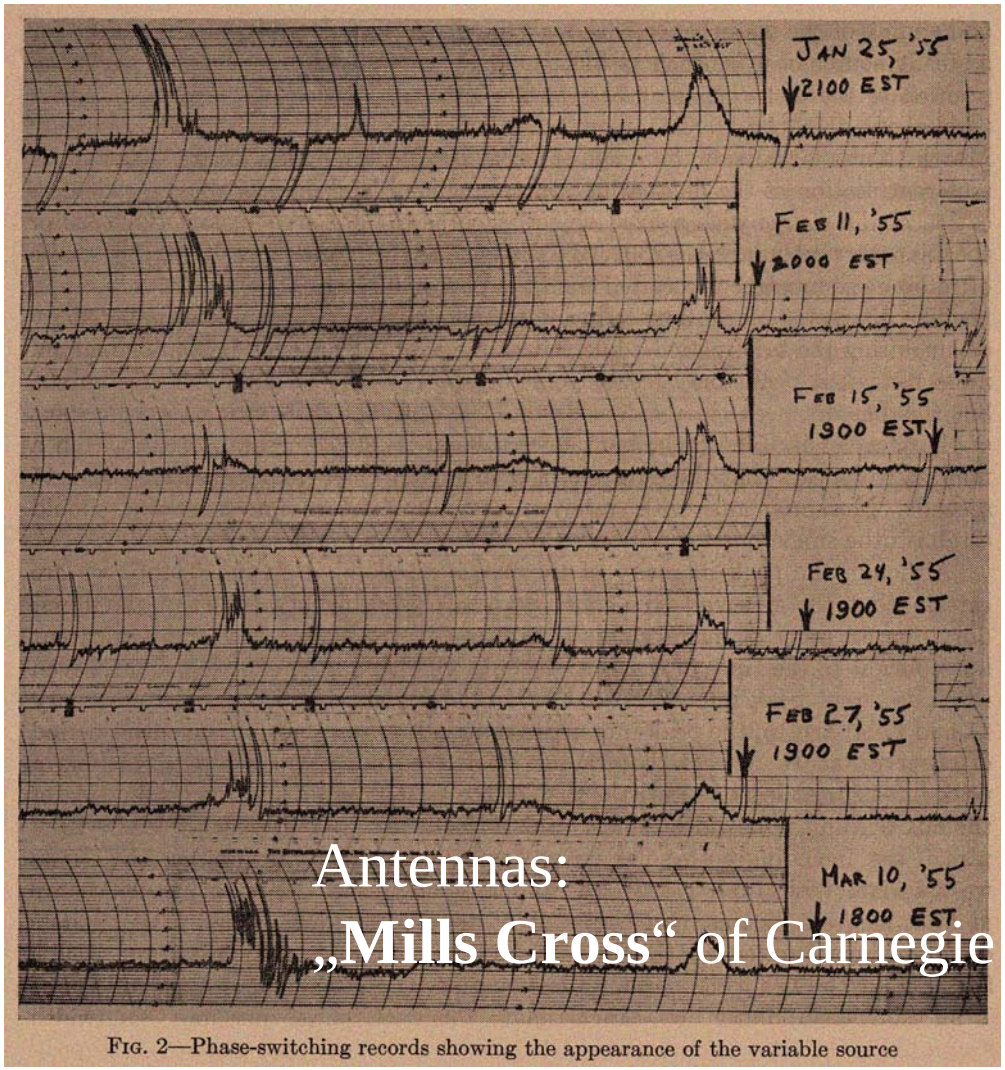

FIG. 2—Phase-switching records showing the appearance of the variable source

Antennas:
„**Mills Cross**“ of Carnegie Institution of Washington

The early days of Planetary Radio Astronomy

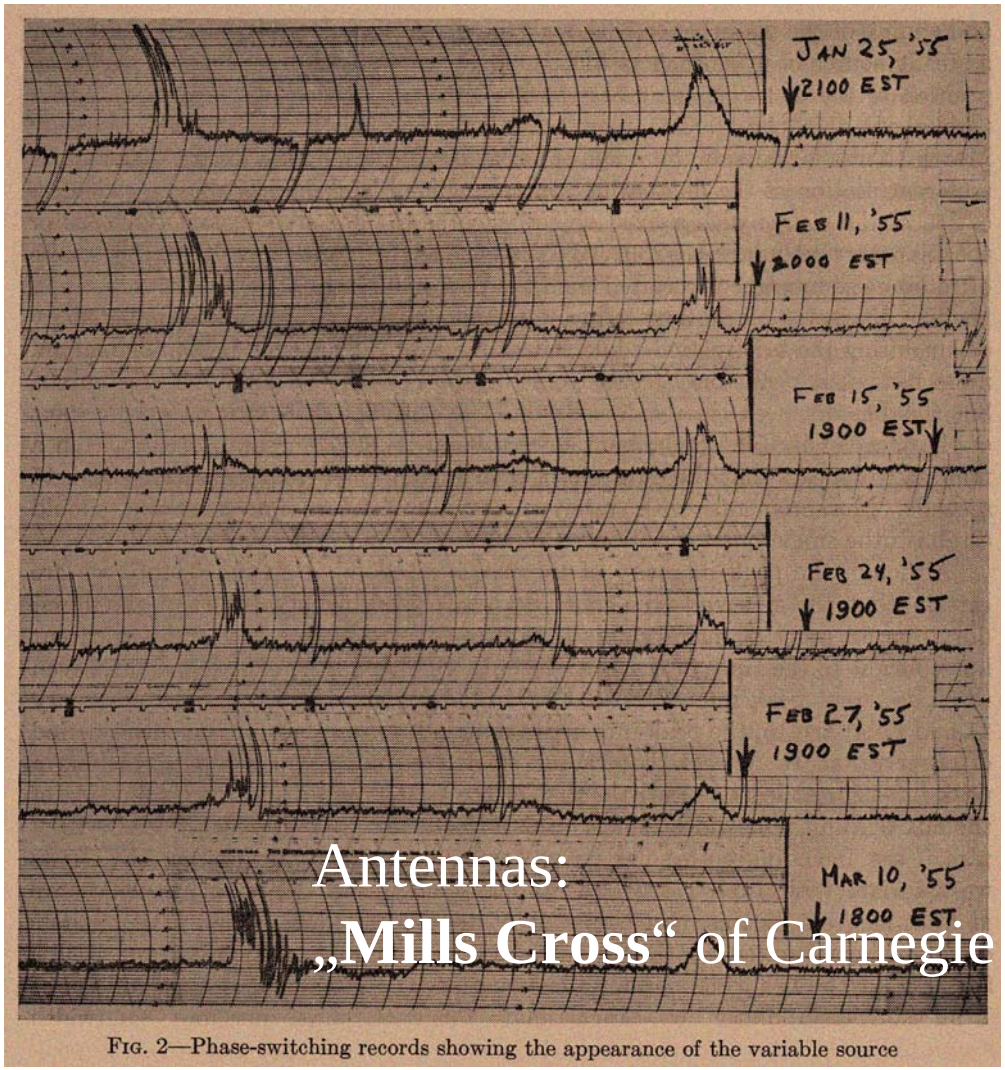

FIG. 2—Phase-switching records showing the appearance of the variable source

3 months of observations
Jan, Feb, March 1955

Antennas:
„**Mills Cross**“ of Carnegie Institution of Washington

The early days of Planetary Radio Astronomy

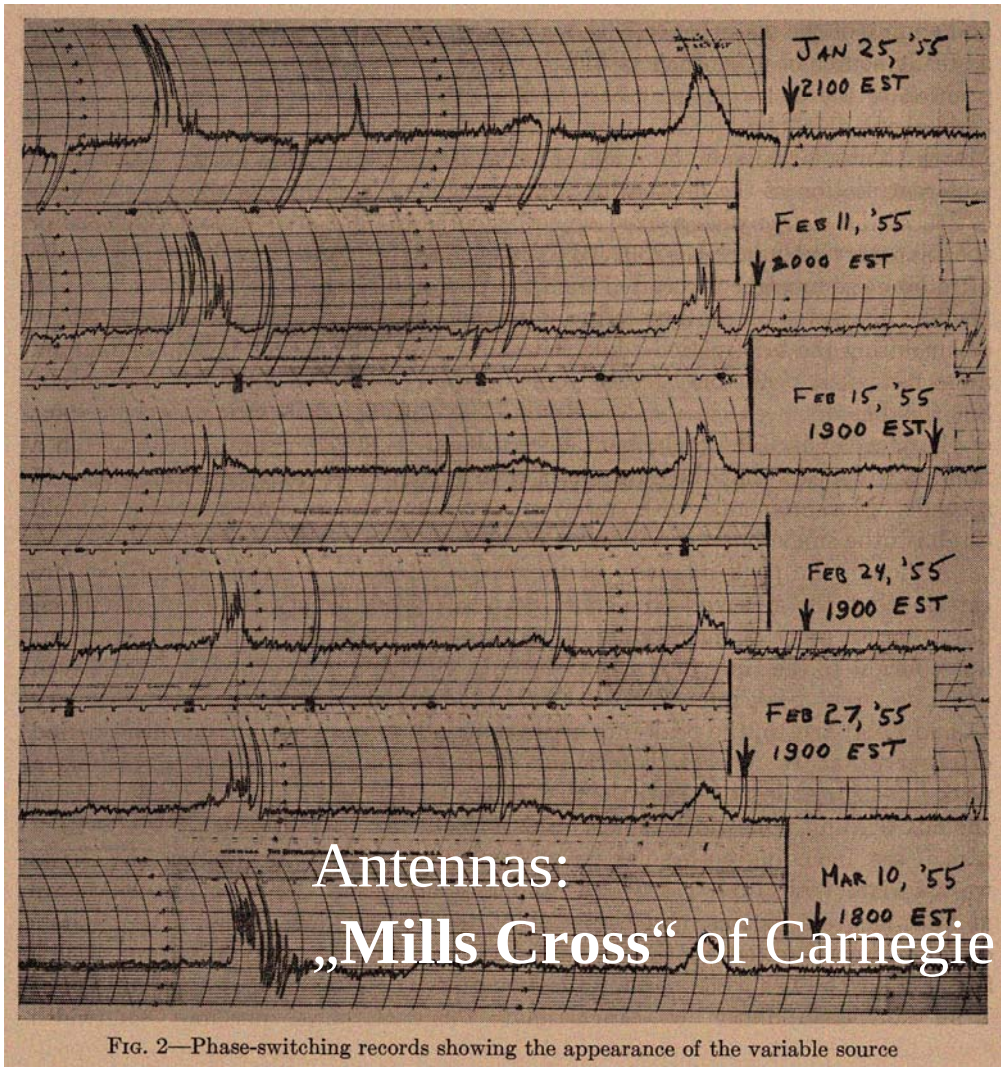

FIG. 2—Phase-switching records showing the appearance of the variable source

3 months of observations
Jan, Feb, March 1955

↓

received by JGR
April 1955

Antennas:
„**Mills Cross**“ of Carnegie Institution of Washington

The early days of Planetary Radio Astronomy

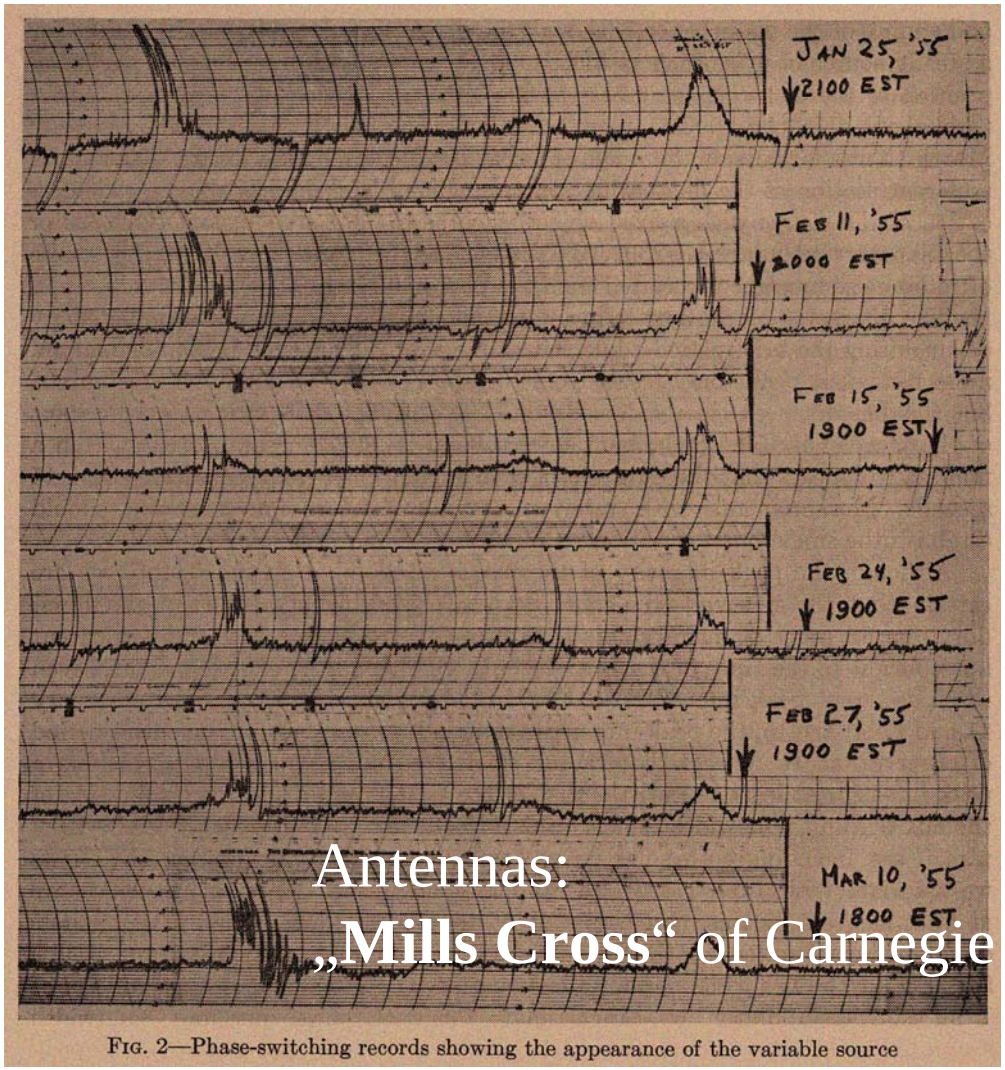

FIG. 2—Phase-switching records showing the appearance of the variable source

3 months of observations
Jan, Feb, March 1955

↓

received by JGR
April 1955

↓

published in June 1955

Antennas:
„**Mills Cross**“ of Carnegie Institution of Washington

The early days of Planetary Radio Astronomy

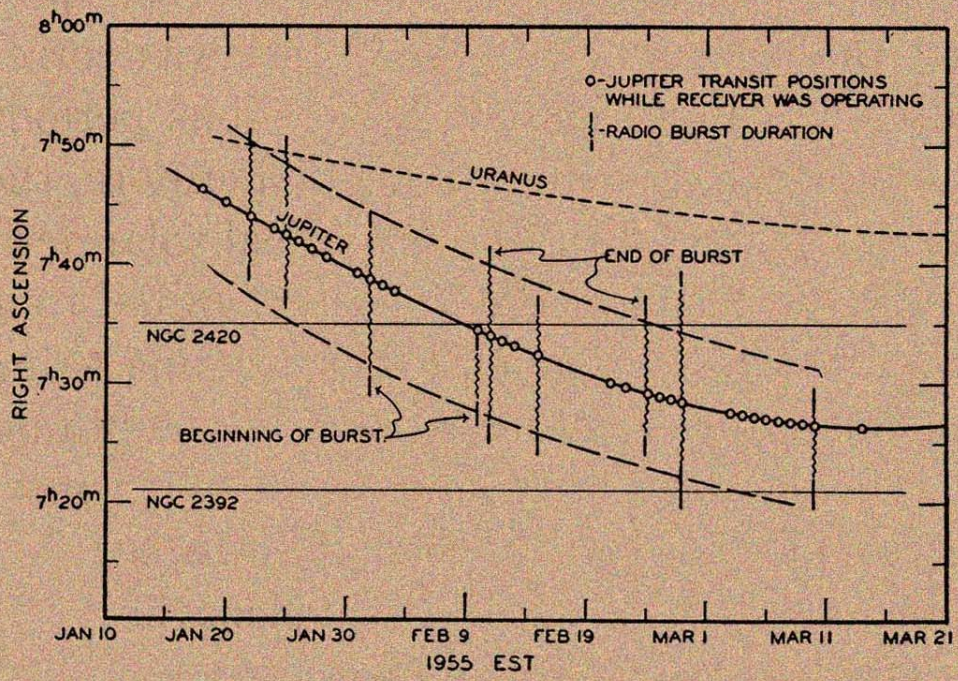

FIG. 3—Comparison of right ascension and duration of bursts with positions of Jupiter, Uranus, and two galactic objects

Radio Modulation

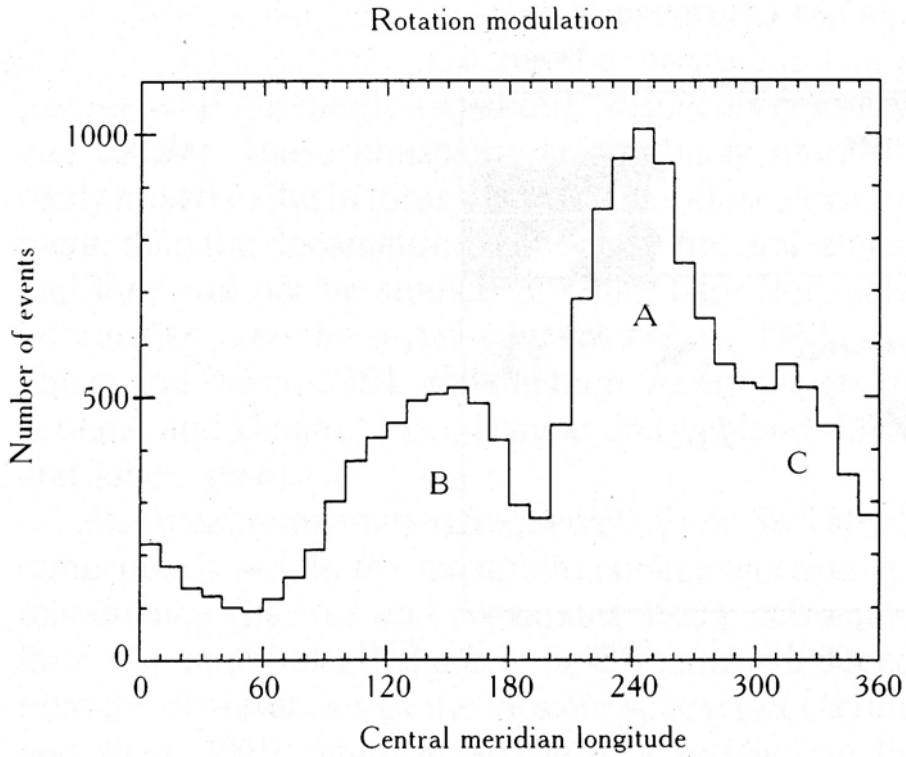

Modulation by planetary rotation

Synoptic decametric observations over long time intervals:

→ rotation period of core of Jupiter

9h 55m 29.71s +/– 0.01s

(Genova et al., 1987: observations at Boulder 1960 - 1975, at Nancay 1978 – 1984; Warwick et al., 1975; Leblanc et al., 1981, 1983; Leblanc and Gerbault, 1987)

Radio Modulation

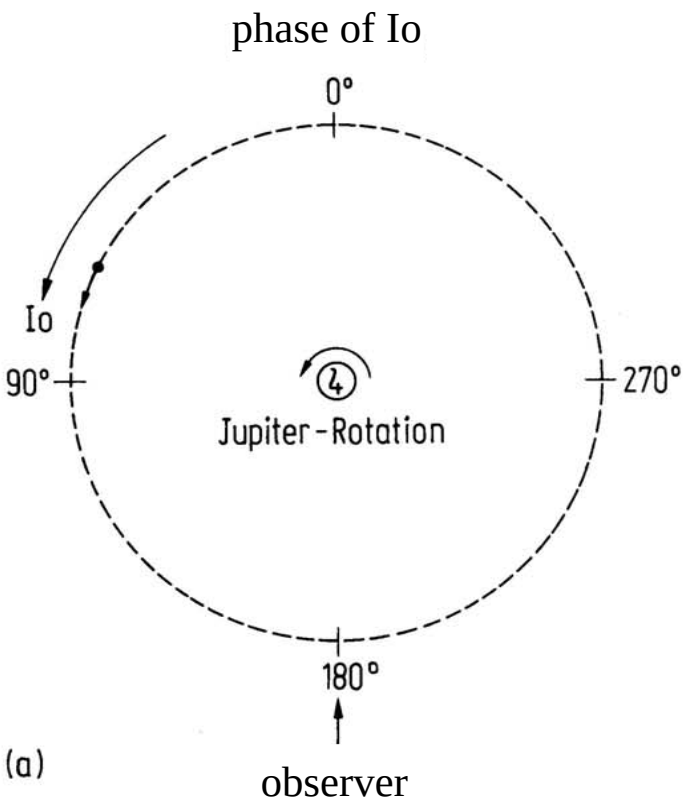

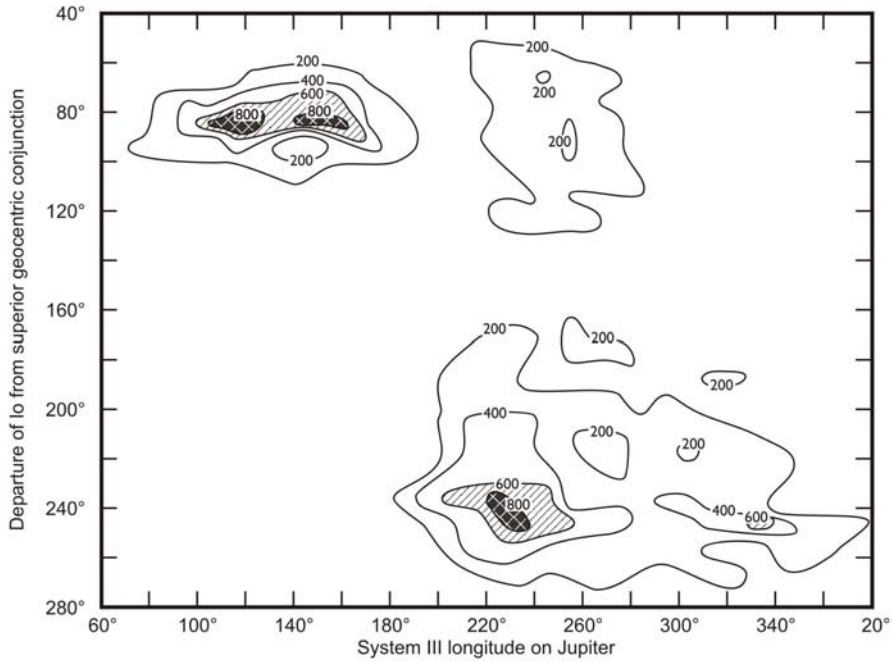

Bigg, E.K. (1964), Influence of the satellite Io on Jupiter‘s decametric emission-. *Nature*, 203: 1008-1010.

Radio Modulation

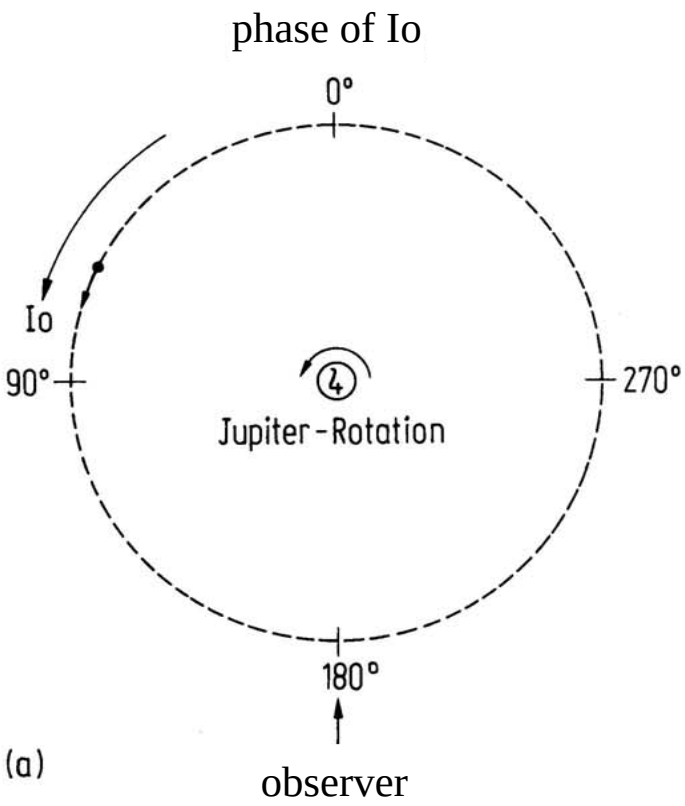

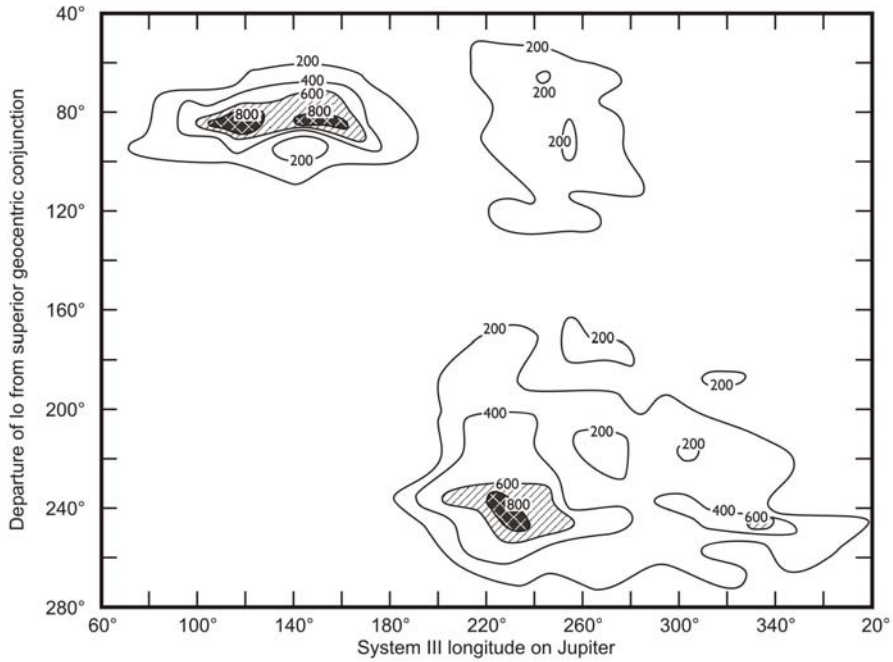

Bigg, E.K. (1964), Influence of the satellite Io on Jupiter‘s decametric emission-. *Nature*, 203: 1008-1010.

Radio Modulation

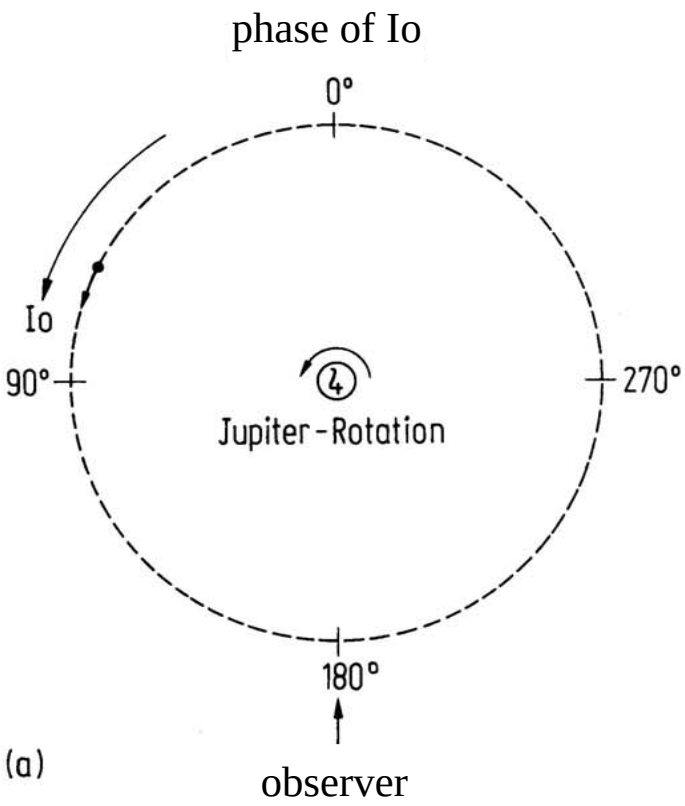

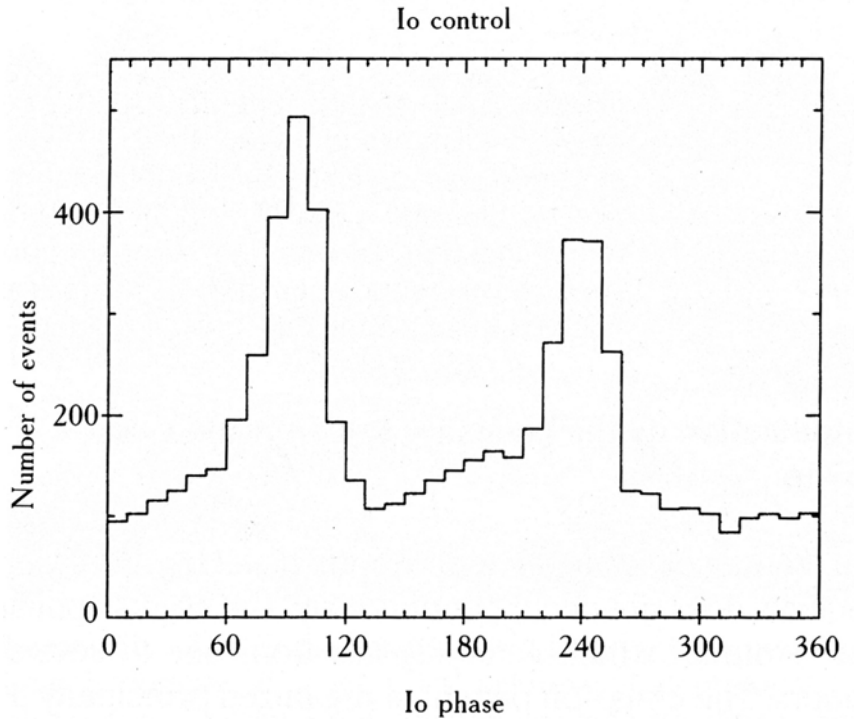

Genova et al., 1987
(Boulder and Nancay observations)

CML–Io Phase Diagram

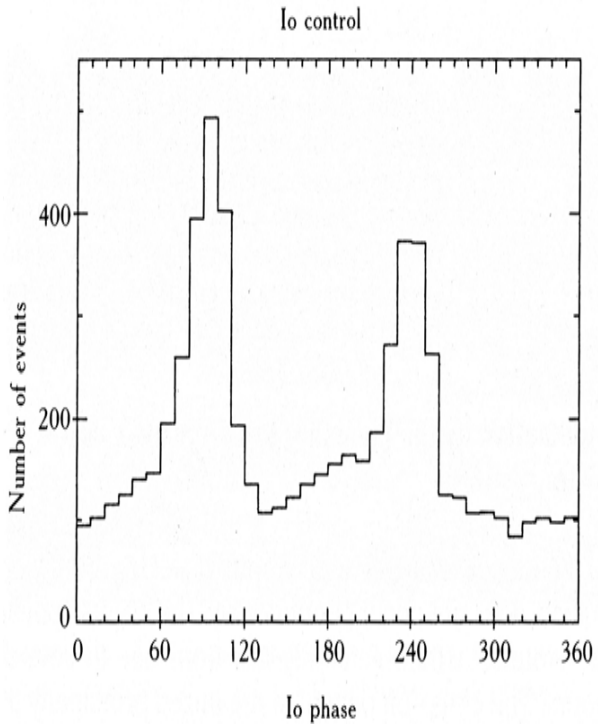

Io-independent

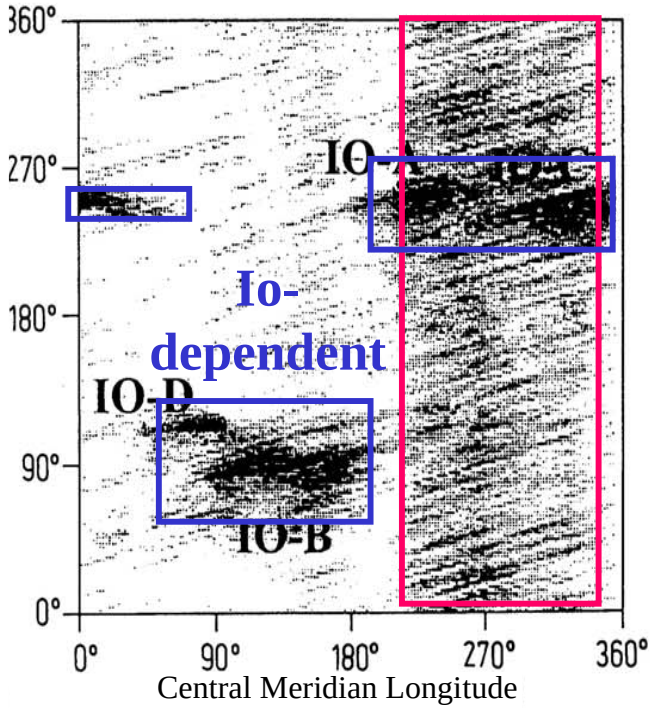

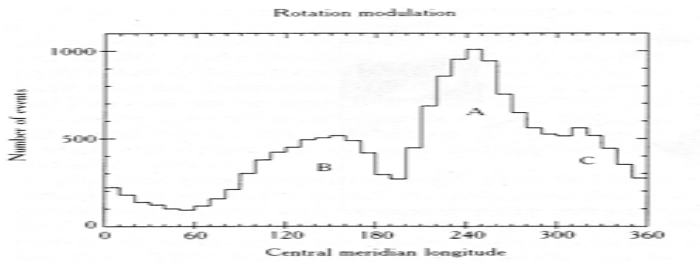

Nature of Radio Emission

Fundamental property of planetary radio emission:

Non-thermal radio emission is mostly generated as emission of gyrating electrons in high latitudes of magnetized planets.

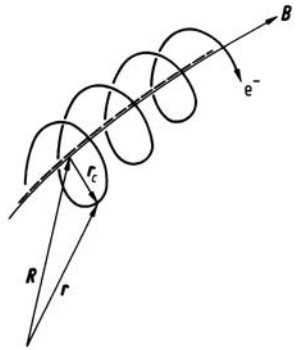

$$f \approx f_{ce}$$

$$f_{ce} = \frac{1}{2\pi}\frac{eB}{m_e}$$

In the case of **Jupiter** at frequencies received on terr. ground, i.e. ~ > 10 MHz: RH (LH) polarized from northern (southern) hemisphere, X-mode (fast extraordinary magneto-ionic) mode, emitted close to its local cut-off frequency: $f \cong f_X$
($f_X \approx f_{ce}$ in a strongly magnetized/depleted plasma)

Jupiter with strongest planetary magnetic field:
Bmax ~ 14 Gauss on northern surface, corresponds to cyclotron freuquency fmax ~ 40 MHz (observable from terrestrial grounds)

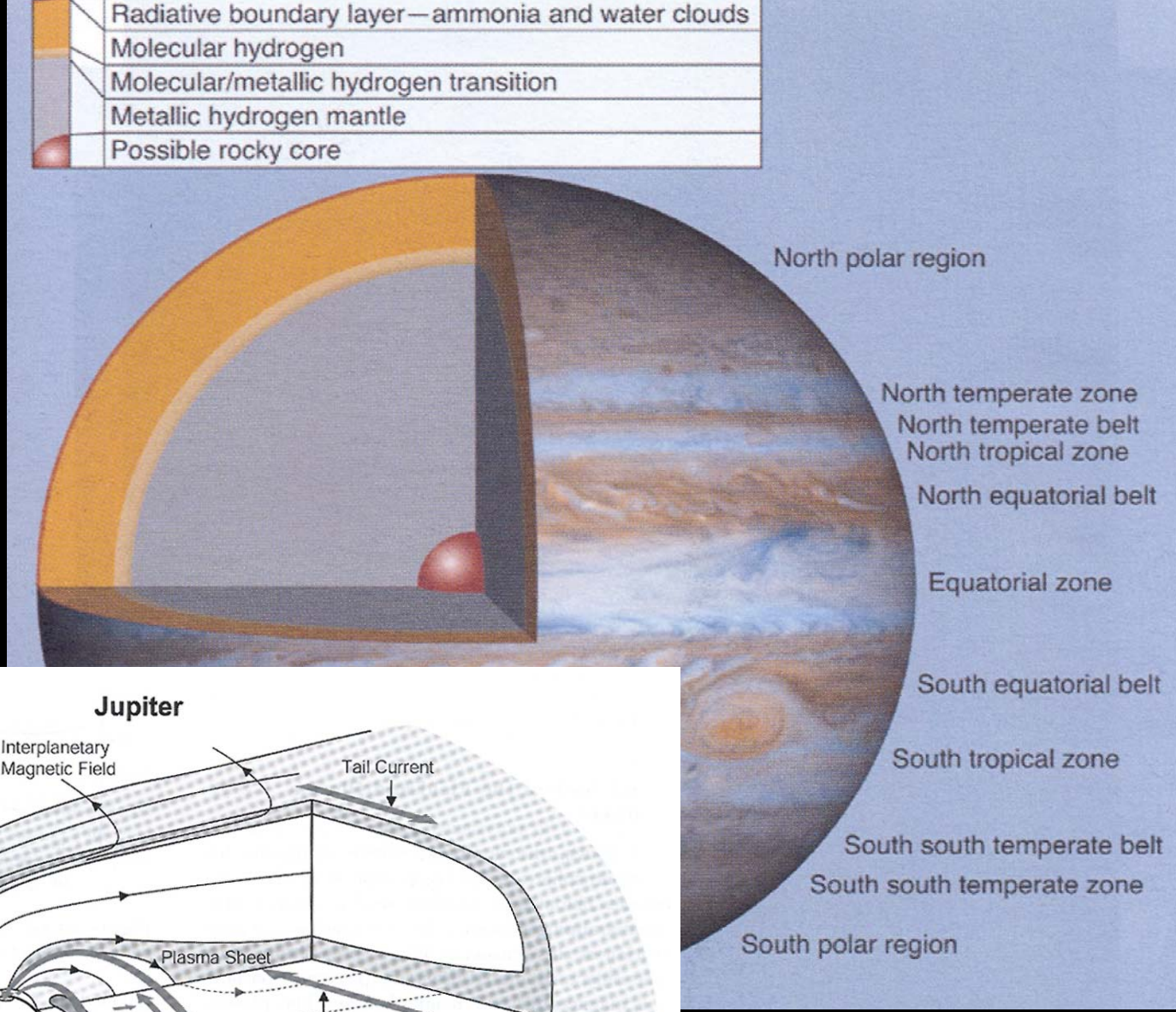

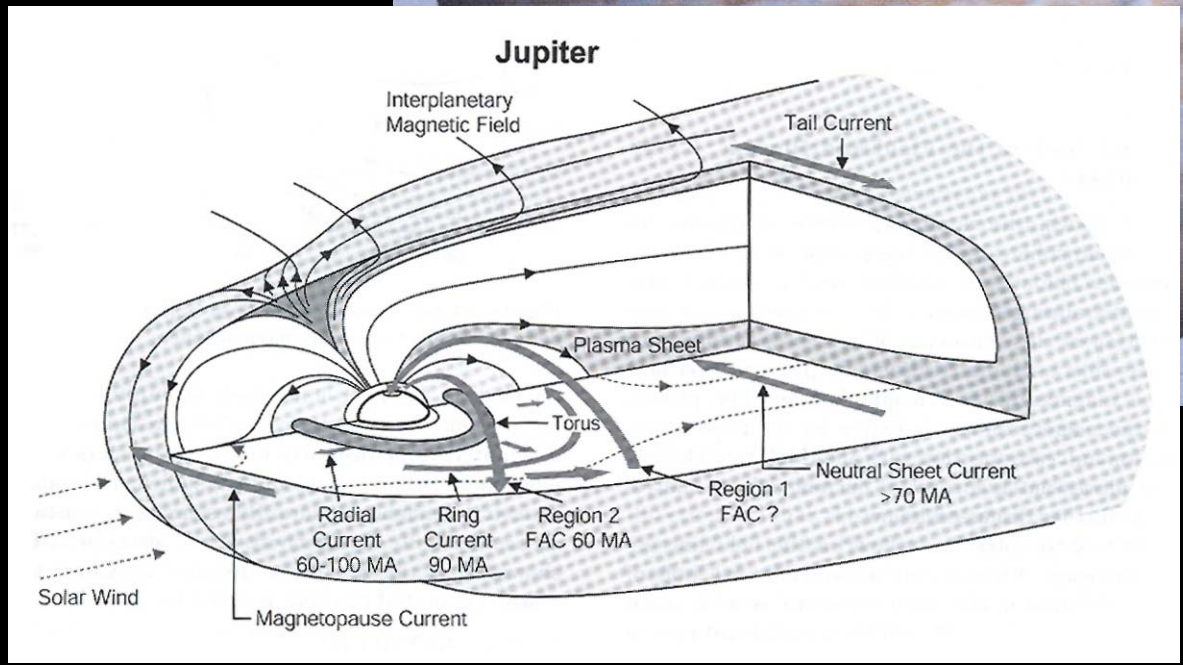

Io – Jupiter Interaction

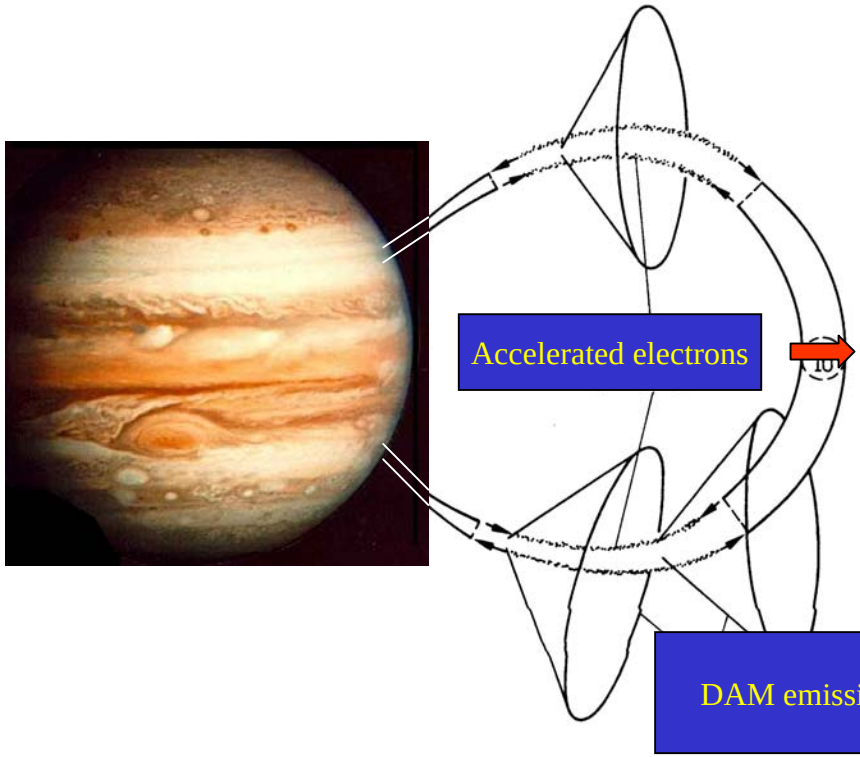

Electric field E at the position of Io across the Io flux tube (IFT):

$$\vec{E} = -\left[\vec{v}_{rel} \times \vec{B}\right]$$

Potential difference across IFT :

$$\Phi \approx 411 kV$$

Decameter Radio Emission from Jupiter

Galilean satellite Io

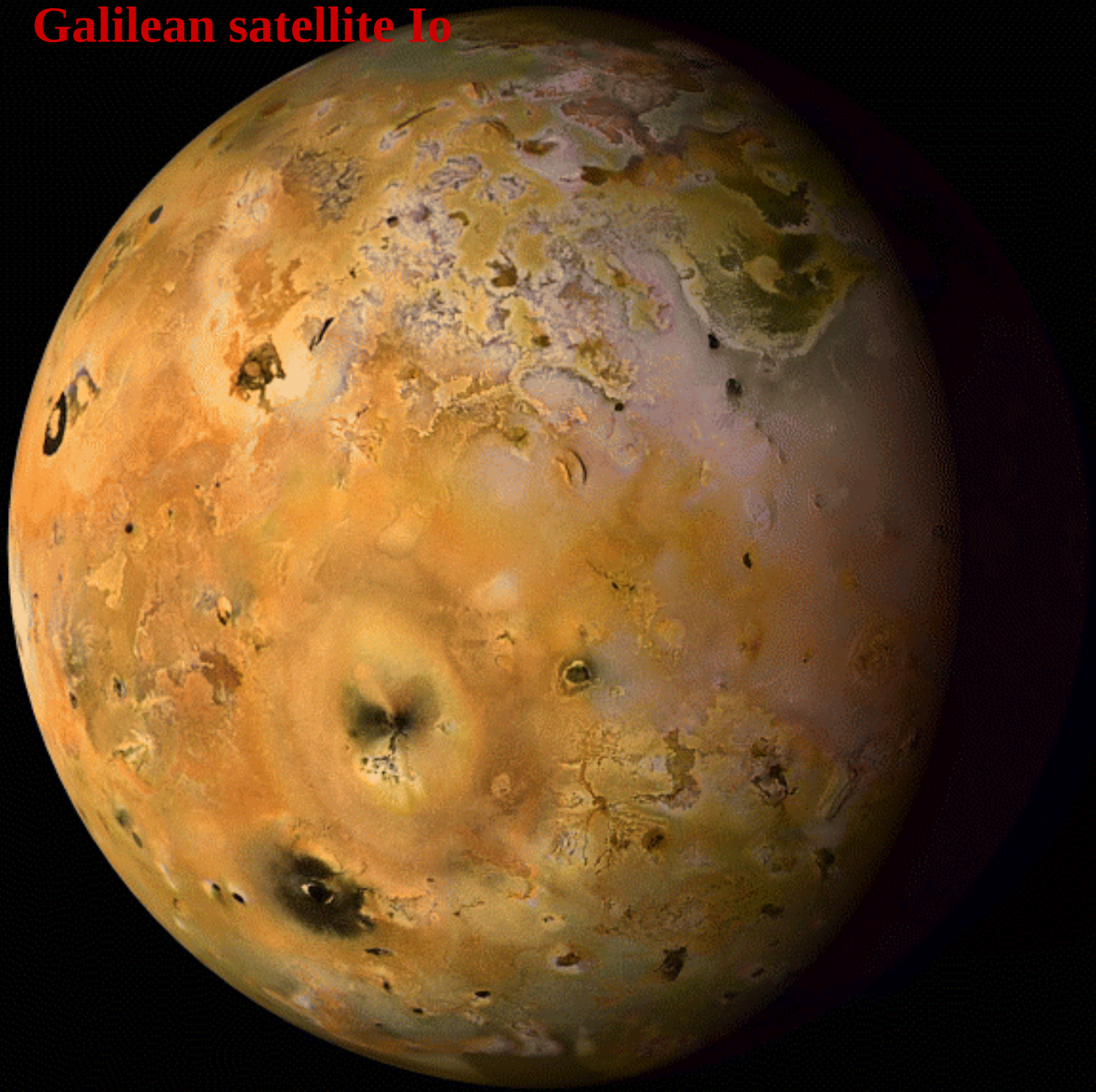

- Volcanoes on Io
- Sputtering of corotating magnetospheric plasma on Io surface
- Conducting layer „ionosphere“

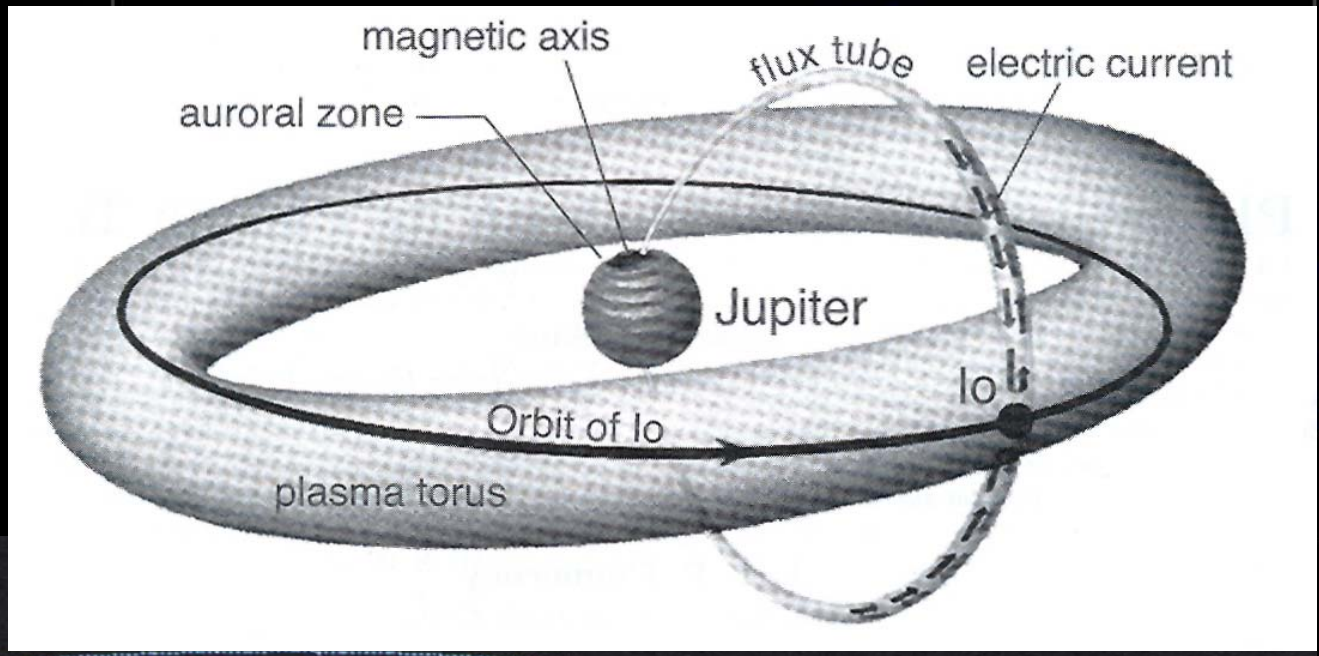

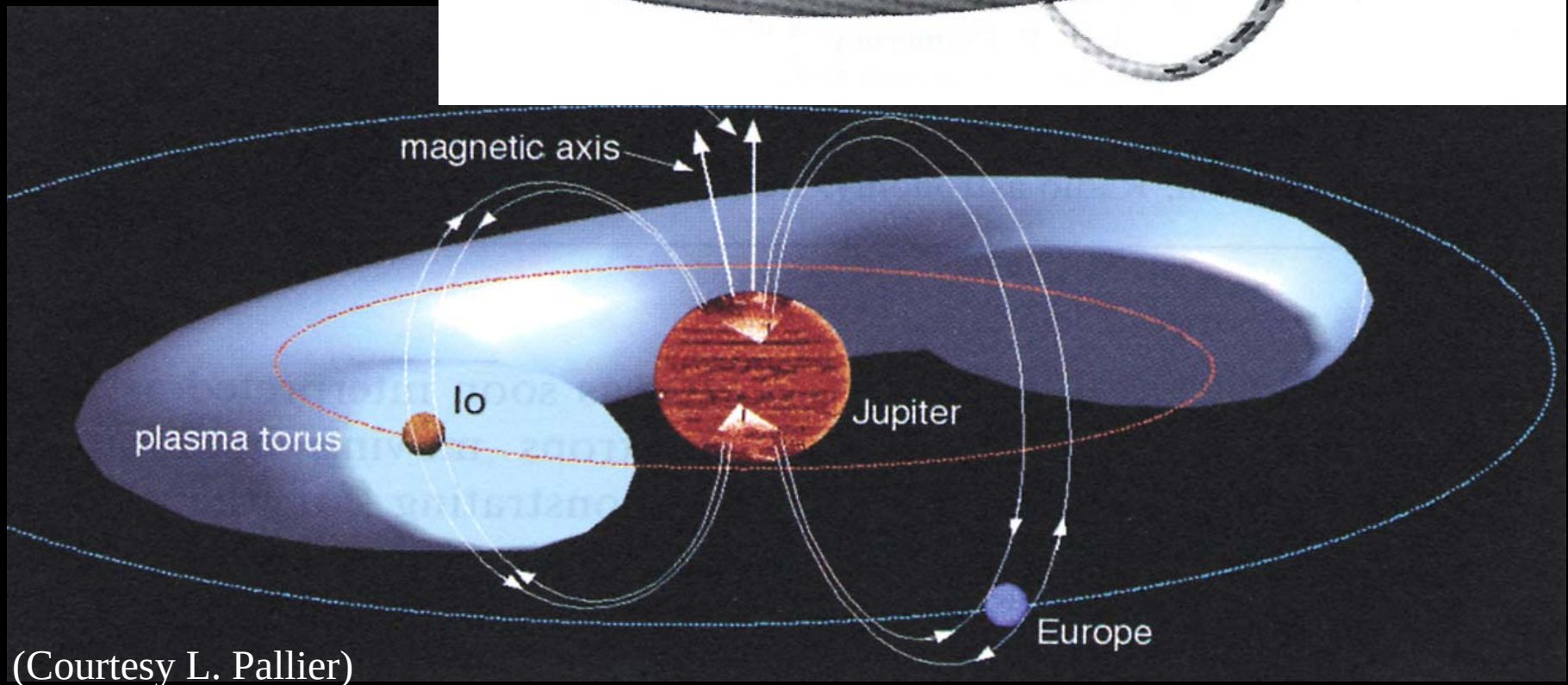

(Courtesy L. Pallier)

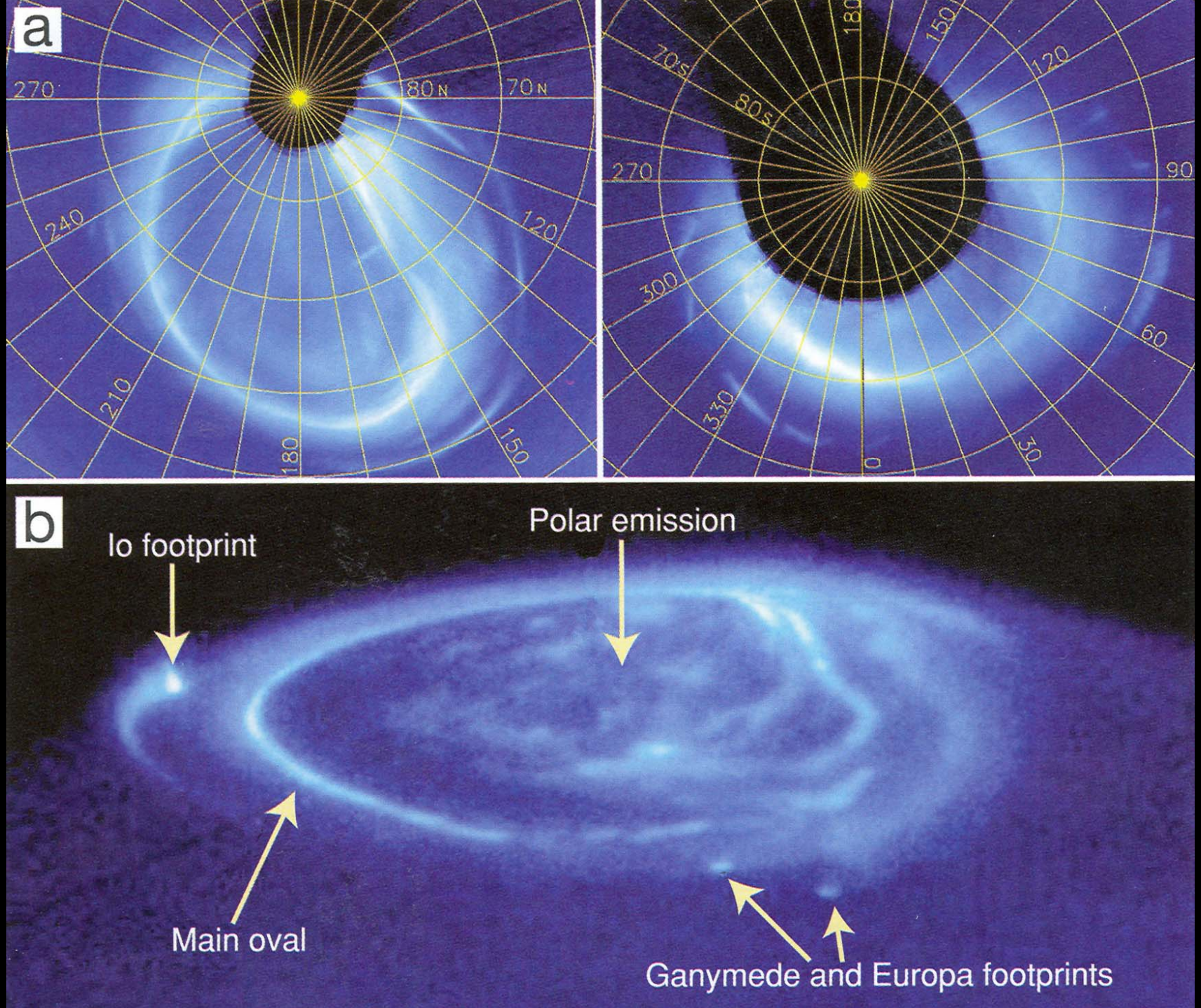
a
270
80 N
70 N
240
120
210
180
150
70 S
80 S
180
150
120
270
90
300
60
330
0
30
b
Io footprint
Polar emission
Main oval
Ganymede and Europa footprints

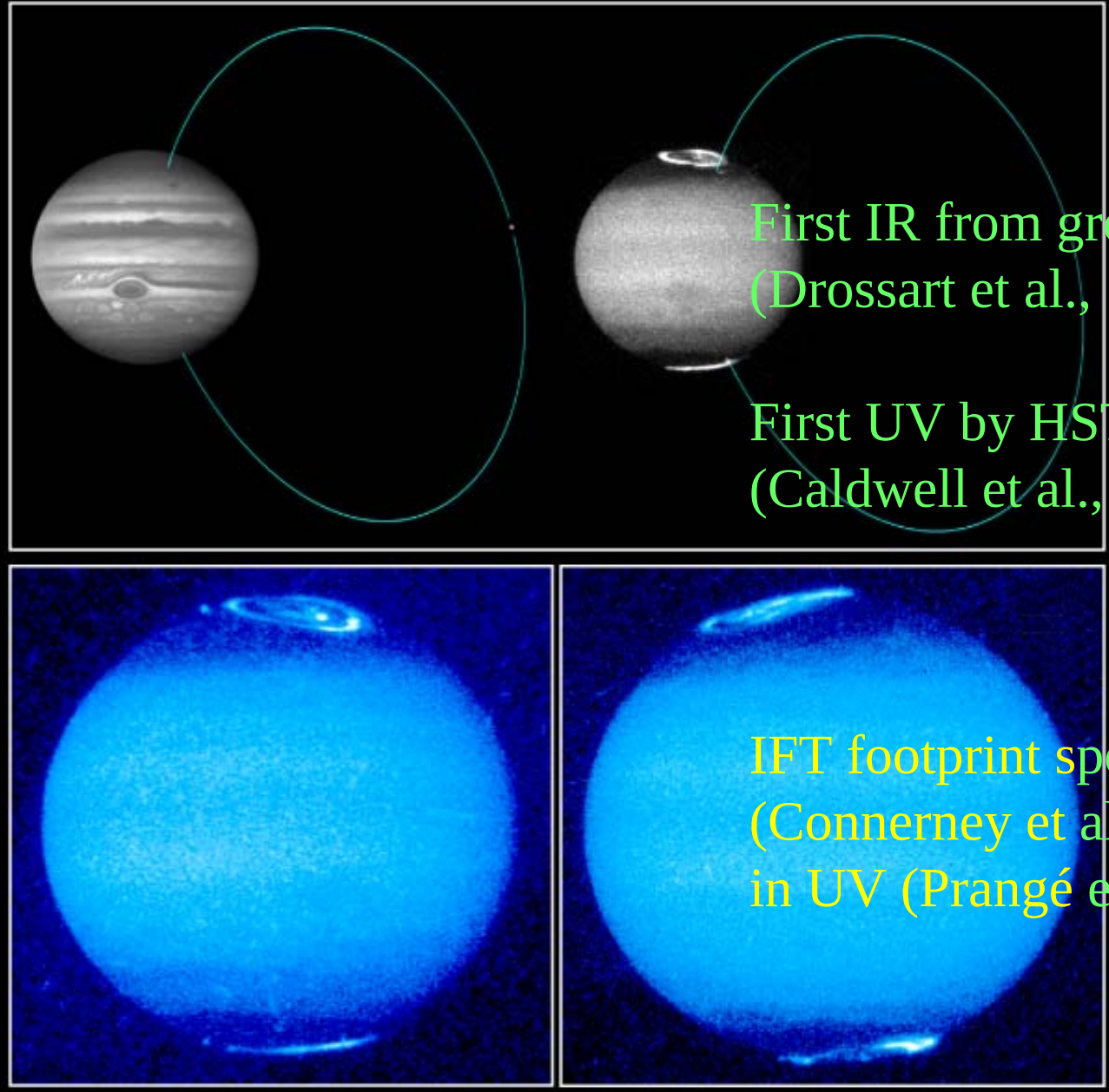

First IR from ground
(Drossart et al., 1992)

First UV by HST
(Caldwell et al., 1992)

IFT footprint spot in IR
(Connerney et al., 1993),
in UV (Prangé et al., 1996)

Jupiter Aurora

HST · WFPC2

PRC96-32 · ST ScI OPO · October 17, 1996
J. Clarke (University of Michigan) and NASA

Dynamic Spectrum of Jupiter Radio Emission

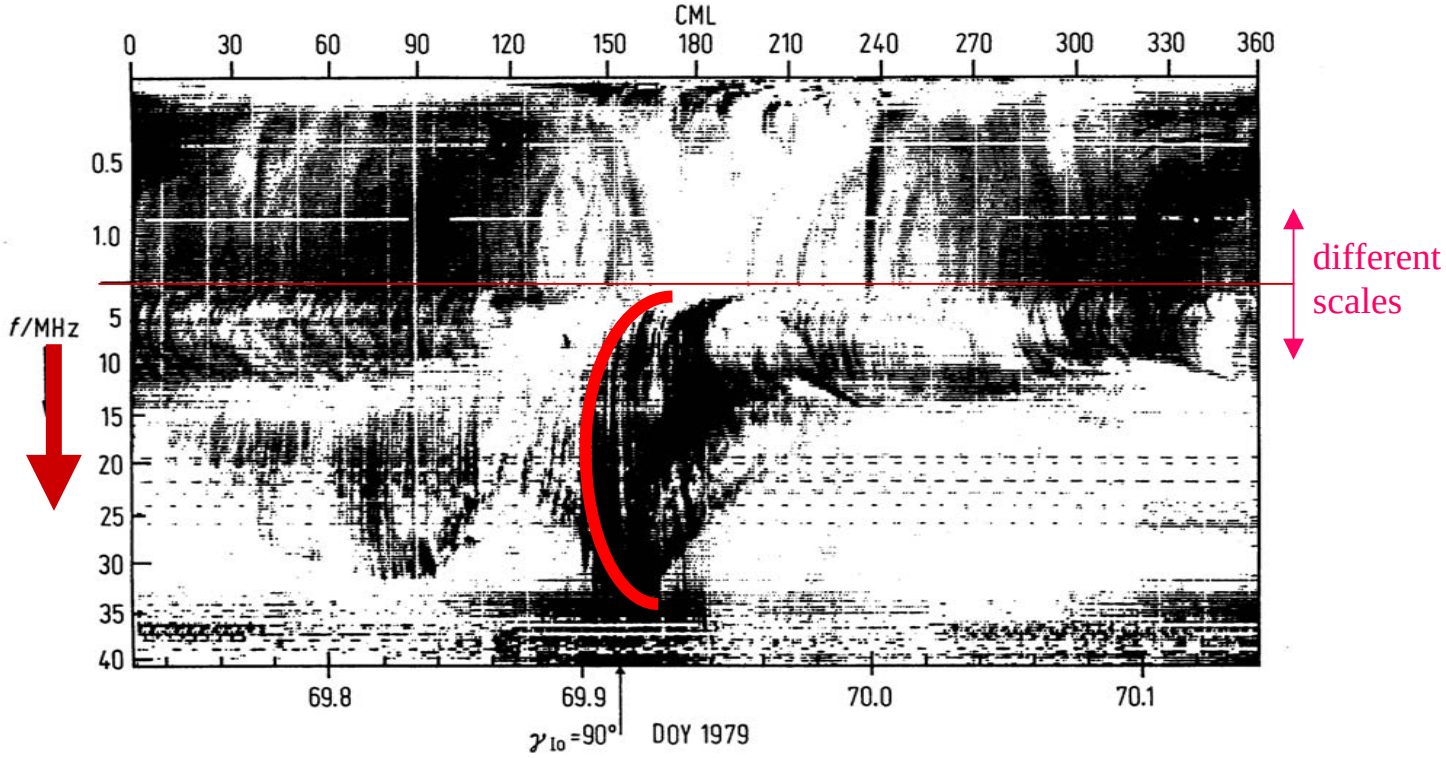

Io-B storm as seen by Voyager 1
after Jupiter closest approach in March 1979

Dynamic Spectrum of Jupiter Radio Emission

Cassini RPWS, September 18, 2000

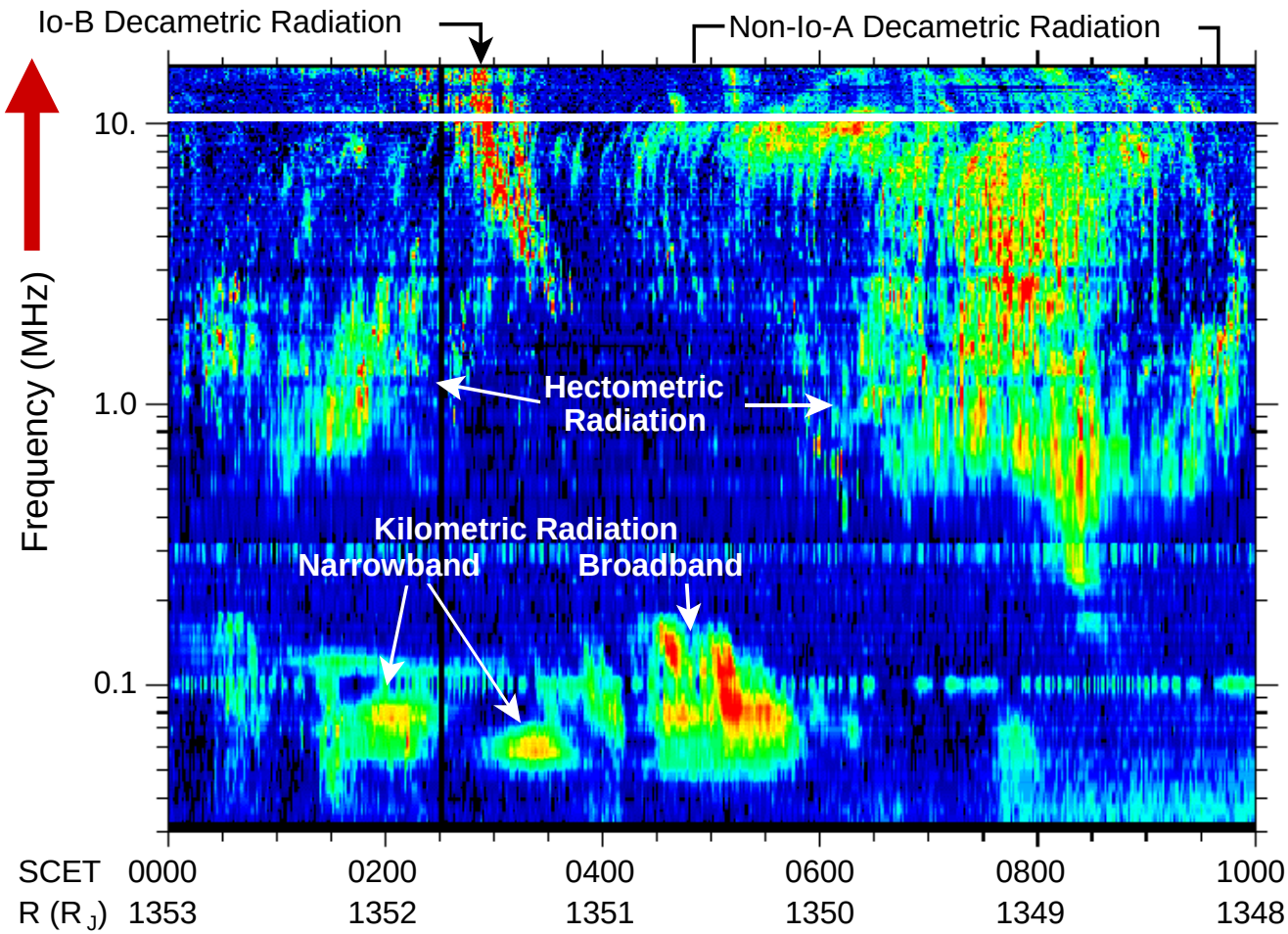

Hierarchy:

- storms
- L-bursts (arcs)
- S-bursts
- sub S-burst structures

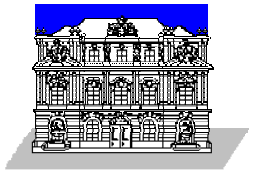

Jupiter Radio Nomenclature

Jovian Radio Components (Kaiser, JGR 1993; Carr et al., 1983)

DIM synchrotron (trapped MeV electrons) ~ 80 MHz–300 GHz

DAM → auroral-DAM → Io-DAM ~ 2 – 40 MHz

(Io-independent) (Io-dependent)

HOM extension into lower frequ. range ~ 0.2 – 2 MHz

KOM → bKOM (auroral zone) ~ 10 – 1000 kHz

→ nKOM (Io torus) ~ 40 – 200 kHz

Continuum, myriametric rad., (outer magnetosph.) ~ 0.1 – 30 kHz

DIM synchrotron (trapped MeV electrons) ~ 80 MHz–300 GHz

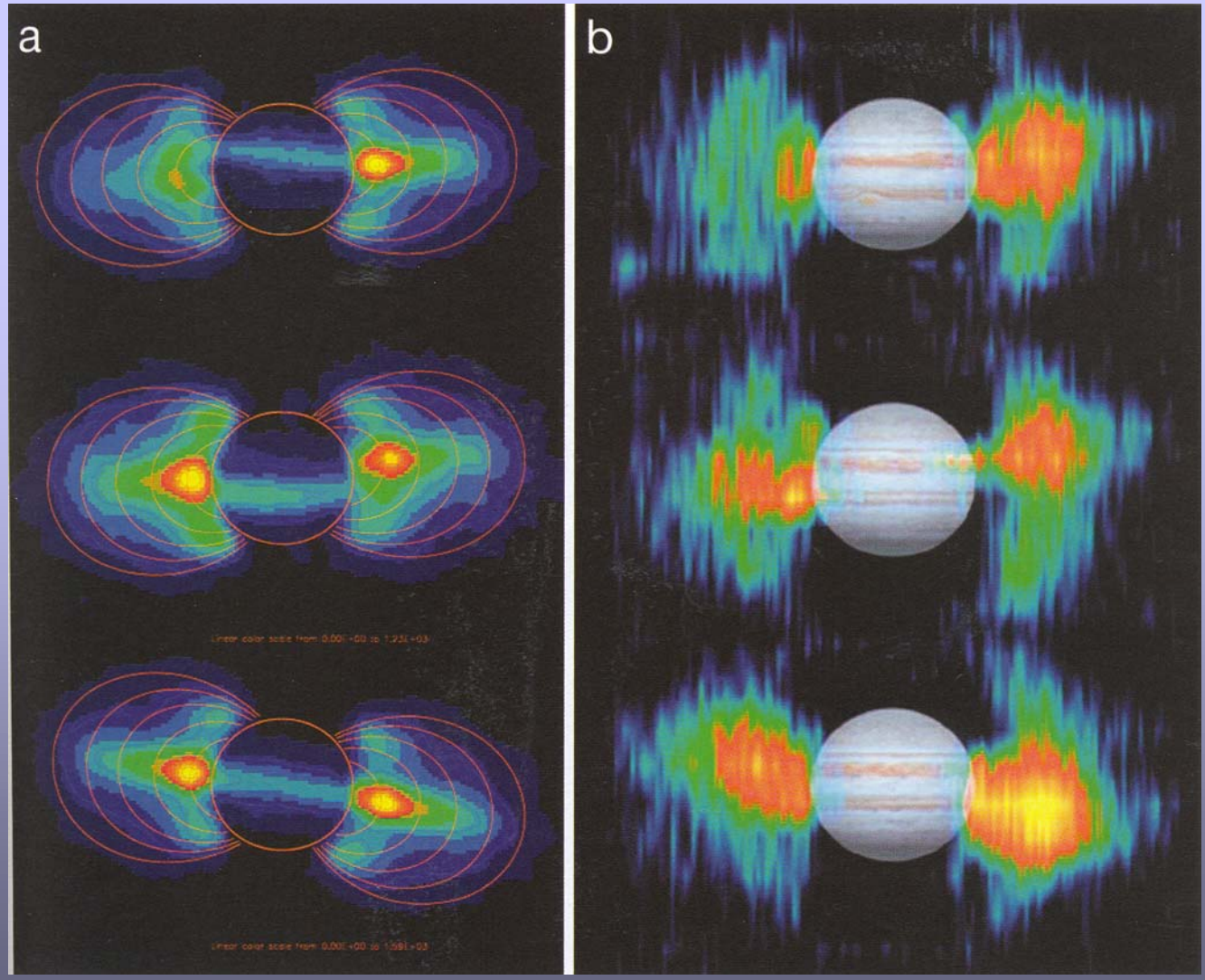

Jupiter Radio Nomenclature

Jovian Radio Components (Kaiser, JGR 1993; Carr et al., 1983)

DIM	synchrotron (trapped MeV electrons)	~ 80 MHz–300 GHz
DAM	→ auroral-DAM (Io-independent) → Io-DAM (Io-dependent)	~ 2 – 40 MHz
HOM	extension into lower frequ. range	~ 0.2 – 2 MHz
KOM	→ bKOM (auroral zone)	~ 10 – 1000 kHz
	→ nKOM (Io torus)	~ 40 – 200 kHz
Continuum, myriametric rad.,	(outer magnetosph.)	~ 0.1 – 30 kHz

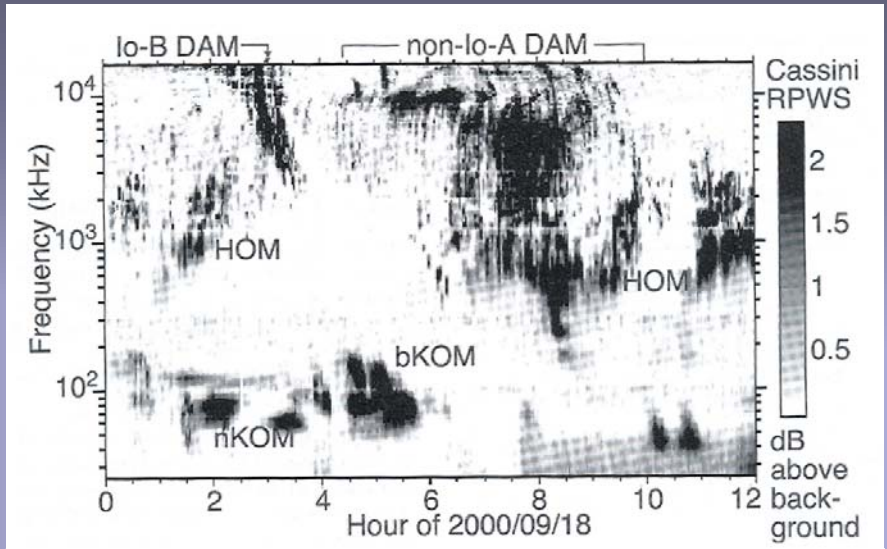

„Zoo“ of Jupiter radio components …

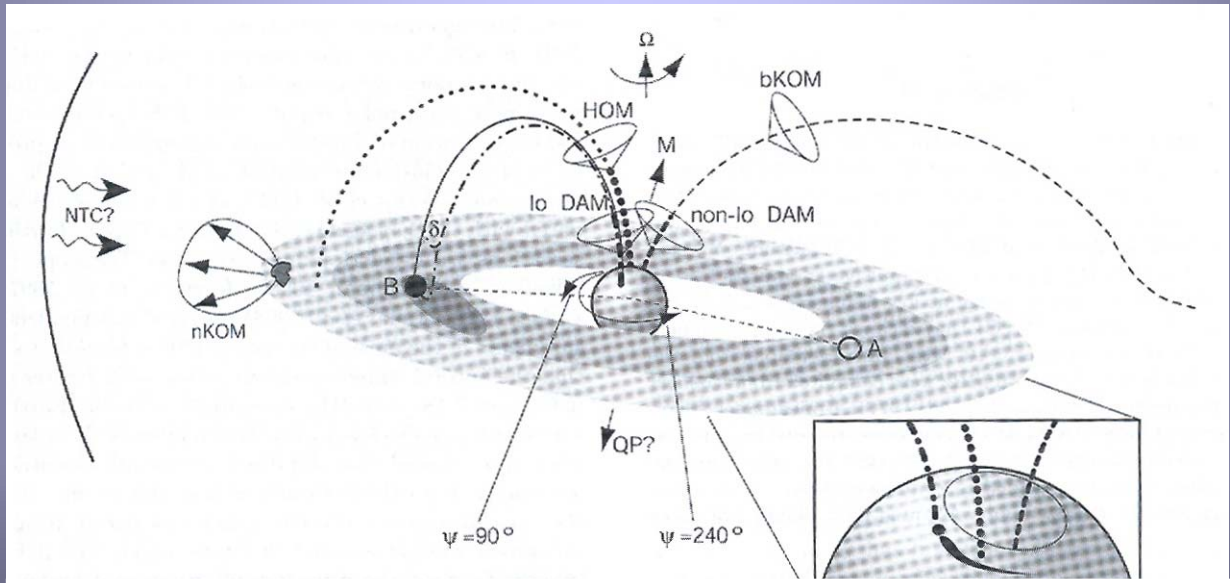

… and their locations in the magnetosphere

Radio Generation Mechanisms

Radio emission from planetary magnetospheres:
Classification of three categories by generation mechanism
(Kurth et al., GRL 24, 2167-2170, 1997)

- Generation by Cyclotron Maser Instability (CMI)

  loss cone distribution: Wu and Lee, ApJ 1979;
  shell distribution: Pottelette et al., JGR 2001;
  Ergun et al., GRL 1998; Treumann, R.A., Planetary radio emission mechanisms, in : Radio Astronomy at Long Wavelengths, Stone et al. (eds.), Geophys.Monograph, vol.119, 13, 2000; Ergun, R.E., PRE VI, 2005.

- Conversion of ES waves into EM waves at $\omega_{uh,res}$

  (linear [e.g. Jones, 1988], nonlinear [e.g. Rönnmark, 1992])

- Emission at $2f_p$ from planetary bow shock

  (Gurnett, 1975)

Cyclotron Maser Mechanism

General dispersion equation for right-handed mode:

$$k^2 - \frac{\omega^2}{c^2} - \frac{\mu_0 e^2}{4\pi m}\omega \iint \frac{\partial f / \partial v_{perp}}{\omega - k_{par} v_{par} - \omega_c / \gamma} v_{perp}^2 dv_{perp} dv_{par} = 0$$

k …wave number

ω… frequency of the wave

ω_c… local gyrofrequency

γ… Lorentz factor

m… electron mass

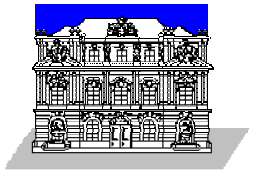

Cyclotron Maser Mechanism

General dispersion equation for right-handed mode:

$$k^2 - \frac{\omega^2}{c^2} - \frac{\mu_0 e^2}{4\pi m}\omega\iint \frac{\partial f / \partial v_{perp}}{\omega - k_{par}v_{par} - \omega_c/\gamma} v_{perp}^2 dv_{perp} dv_{par} = 0$$

$$\omega = \omega_r + i\omega_i$$

$$\omega \in C$$

$$\omega_r, \omega_i \in R$$

Imaginary part of wave = growth rate

$$\omega_i = \frac{\omega_p^2}{8}\int_0^{+\infty} v_{perp}^2 dv_{perp} \int_{-\infty}^{+\infty} \frac{\partial f}{\partial v_{perp}} \partial(\omega_r - k_{par}v_{par} - \frac{\omega_c}{\gamma}) dv_{par}$$

ω_p ..... plasma frequency

$\partial(\,function\,)$ … Dirac function

Cyclotron Maser Mechanism

Auroral Kilometric Radiation, AKR

Electron velocity distribution outside of AKR source region

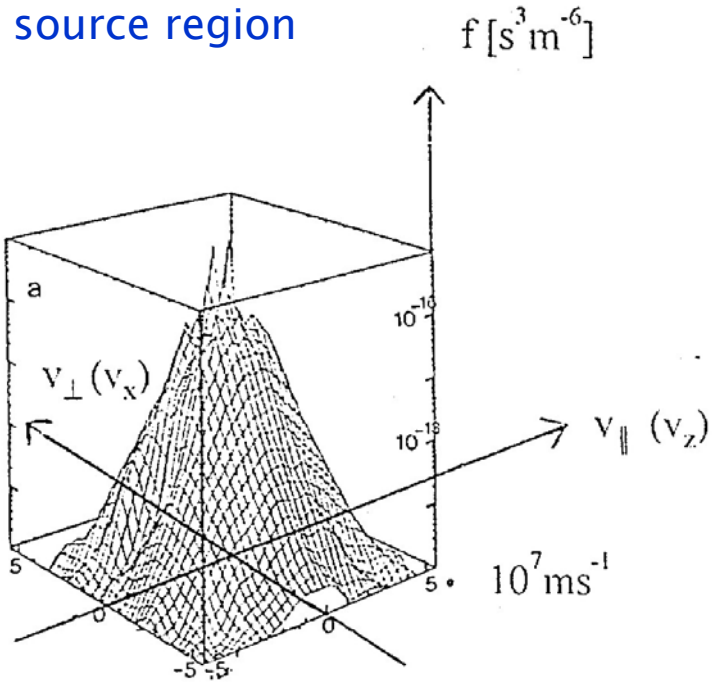

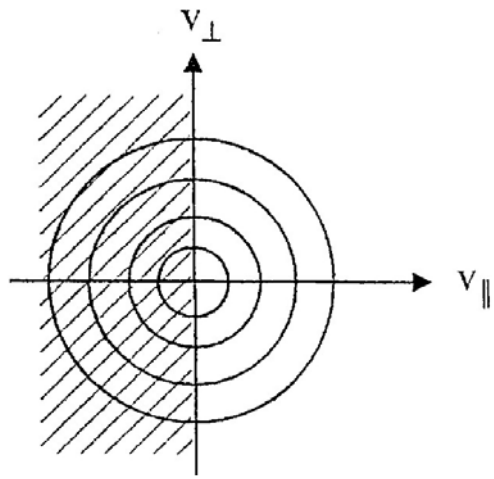

Cyclotron Maser Mechanism

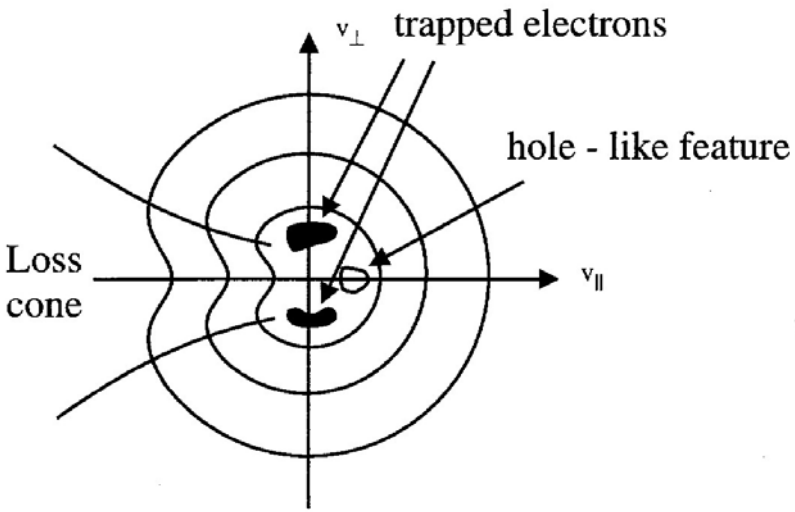

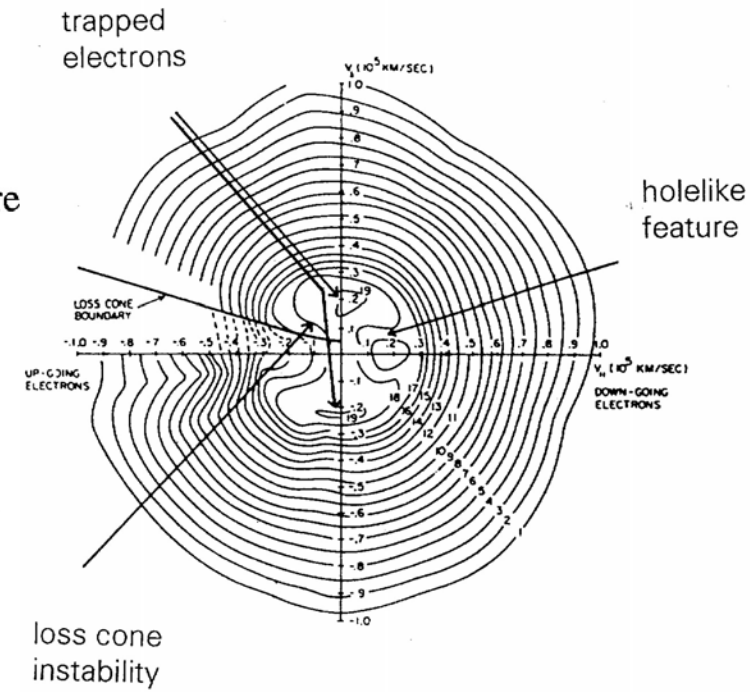

$f(v)$	$s^3\,km^{-6}$
1	0.100 E-4
2	0.215 E-4
3	0.464 E-4
4	0.100 E-3
⋮	⋮
7	0.100 E-2
⋮	⋮
10	0.100 E-1
⋮	⋮
13	0.100 E 0
⋮	⋮
16	0.100 E+1
⋮	⋮
19	0.100 E+2

Electron distribution function, S 3-3 satelite
(Croley et al., JGR 83, 2701, 1978)

Cyclotron Maser Mechanism

Auroral Kilometric Radiation, AKR

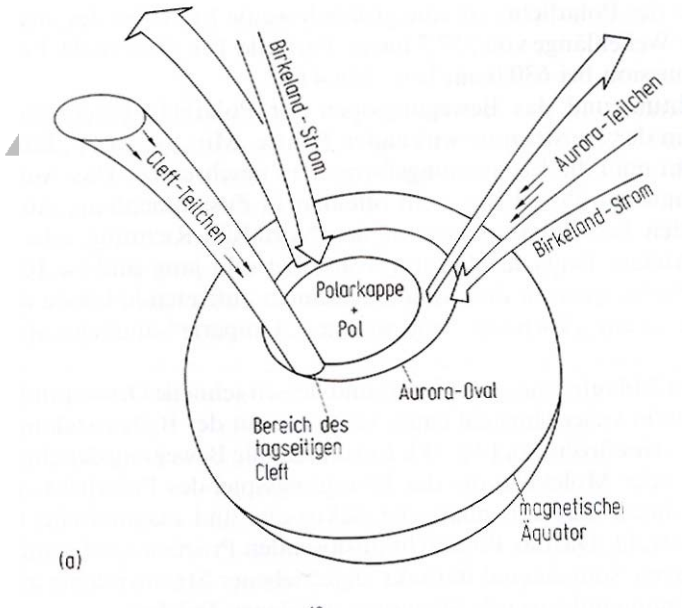

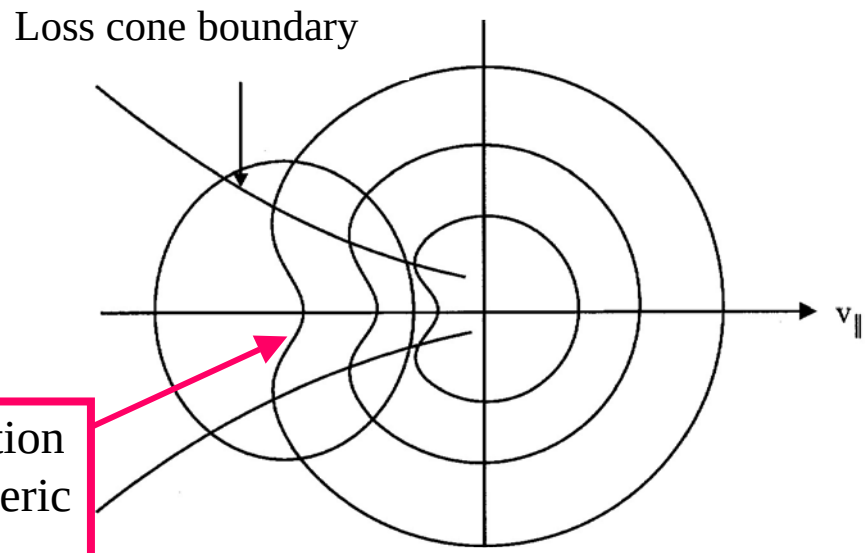

Deviation from Maxwellian distribution due to electron loss by high atmospheric particle collisions.

Cyclotron Maser Mechanism

Electron distribution
Within the AKR source

Electrons with
energies < 1 keV
not considered

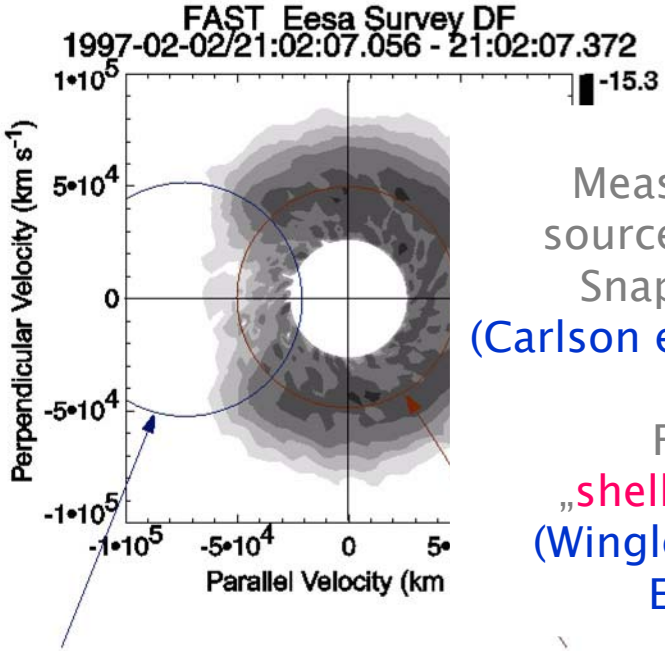

Measurements within AKR source region by Fast Auroral SnapshoT (FAST) Satellite:
(Carlson et al., 1998 and references)

Freee energy from
„shell electron distribution“
(Winglee and Pritchett, 1986;
Ergun et al., 2001)

Loss-cone maser → **Contour 1**
Loss-cone Instability
$k_{\|} = -2.3 \times 10^{-3}\ m^{-1}$
$f = f_{ce} + 5$ kHz
$f_{ce} = 380.3$ kHz

Contour 2
Shell Instability
$k_{\|} = 0$
$f = f_{ce} - 4$ kHz
$f_{ce} = 380.3$ kHz ← Shell maser

Terrestrial Radio Emission: AKR
(Ergun et al., PRE V, 271, 2001)

Wave Generation: Summary

Cyclotron Maser Instability as generation-and wave amplification mechanism

(Wu and Lee, Astrophys. J., 230, 621, 1979)

Particles in regions of velocity distribution with

$$\partial f / \partial v_{par} > 0 \quad \text{and} \quad \partial f / \partial v_{perp} > 0$$

have „free“ kinetic energy for transformation in electromagnetic wave energy

Resonance condition with consideration of relativistic effect

Maximum amplification for R-X mode

ISS

The proof of direct and in-situ observations of a radio source is at present only possible at Earth.

Courtesy Schreiber

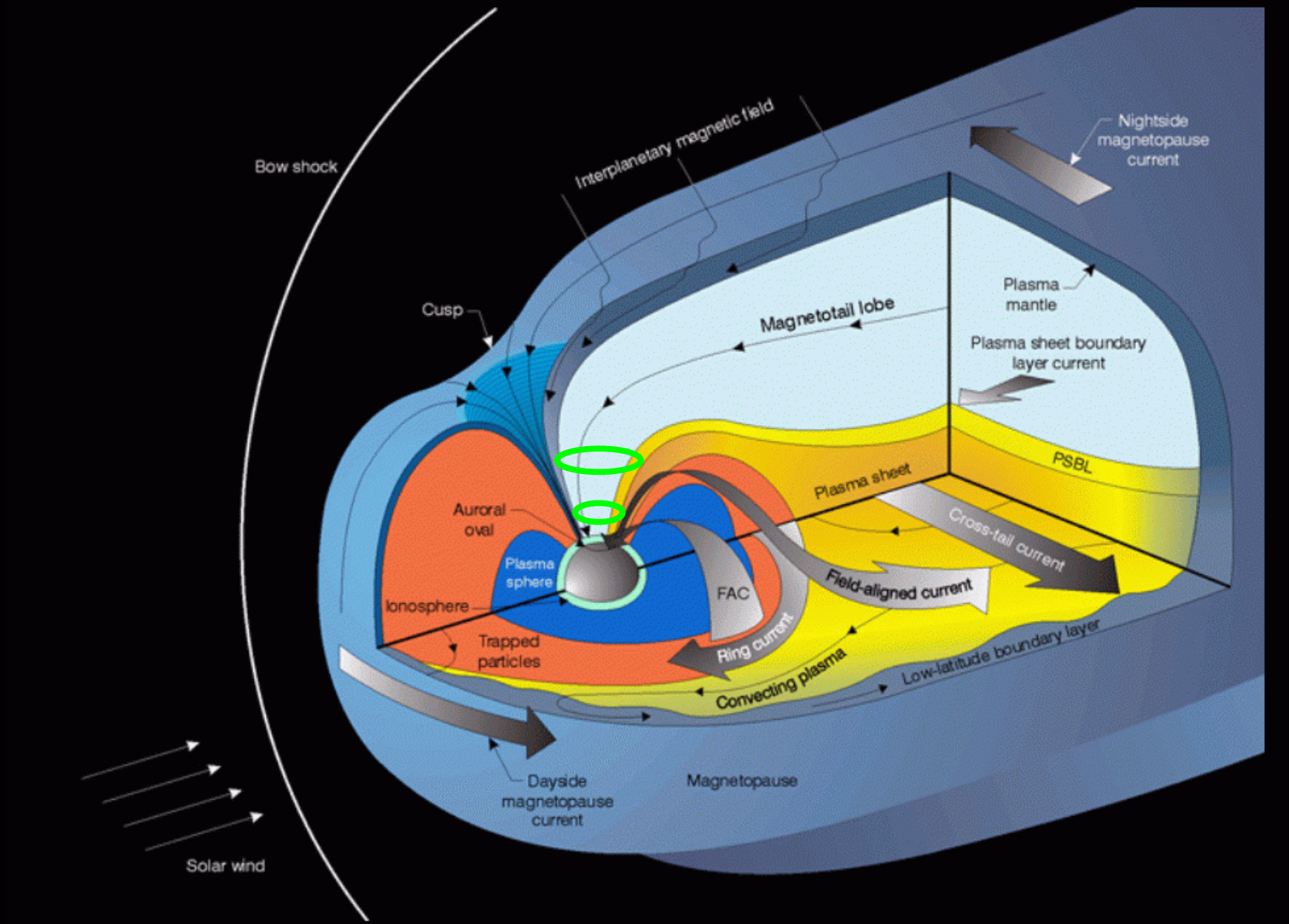

Courtesy Schreiber

Auroral Kilometric Radiation (AKR): source and related oval feature

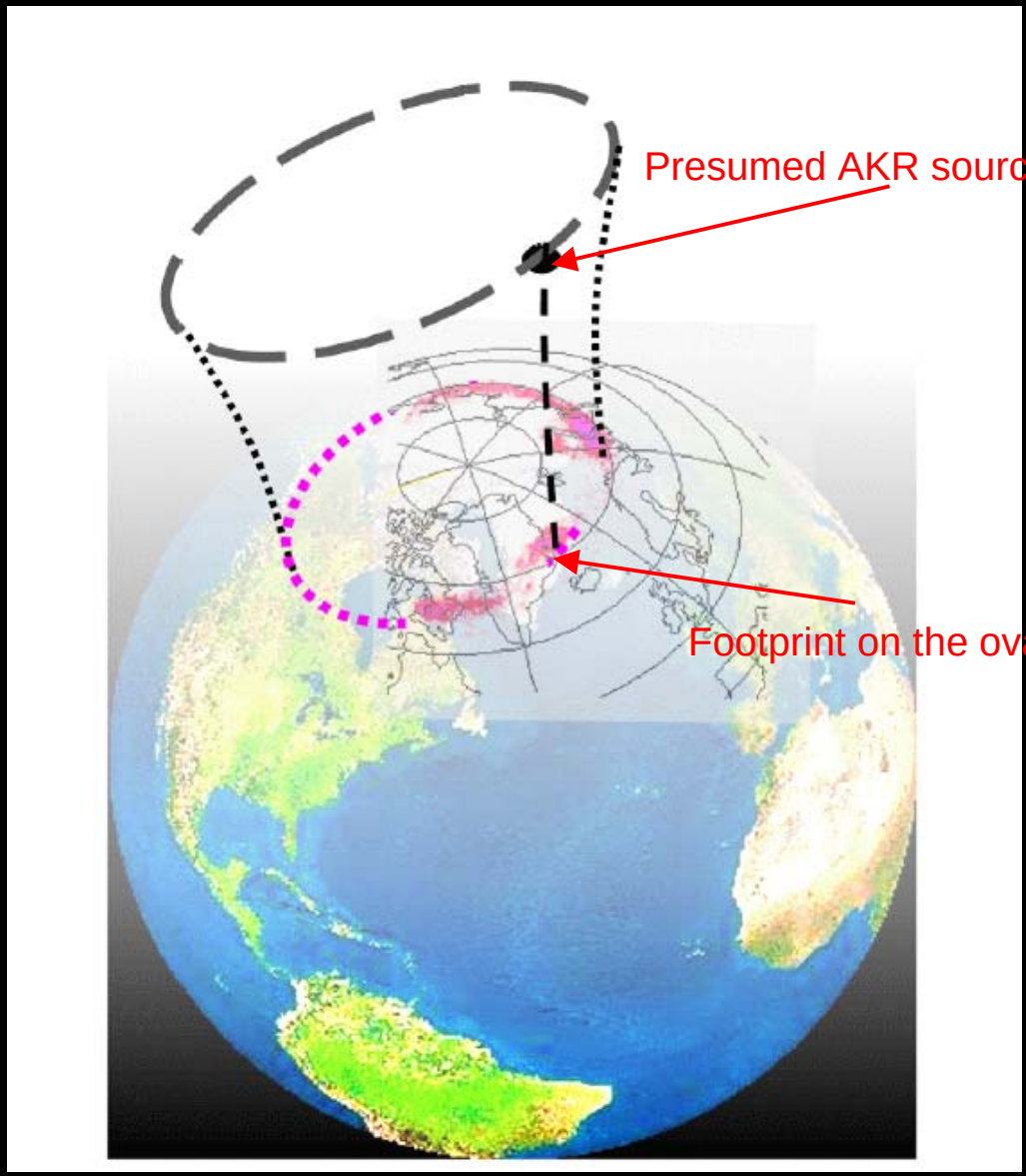

adapted from Mutel et al., 2003

Courtesy Schreiber

Hollow Cone Model

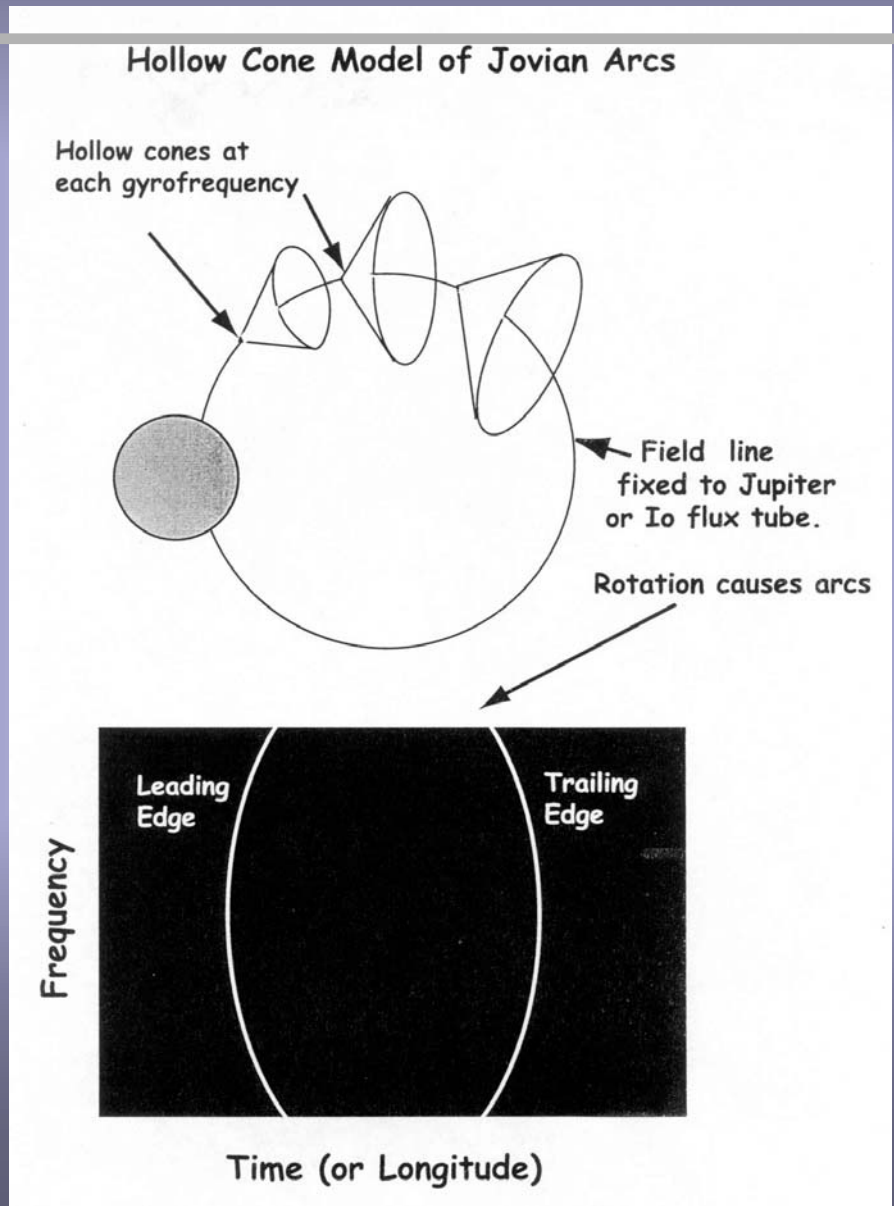

(Kaiser et al., 2000)

Hollow Cone Model

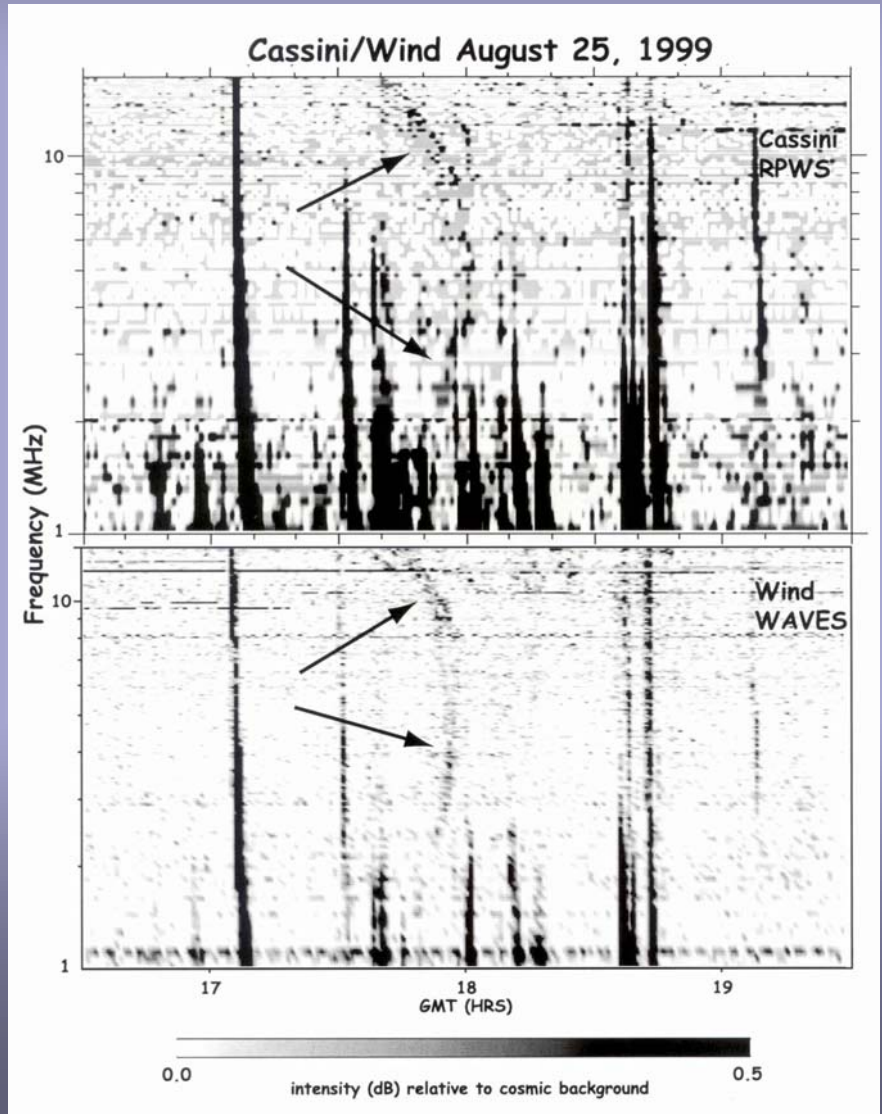

Proof by simultaneous Wind and Cassini measurements

(Kaiser et al., 2000)

Hollow Cone Model

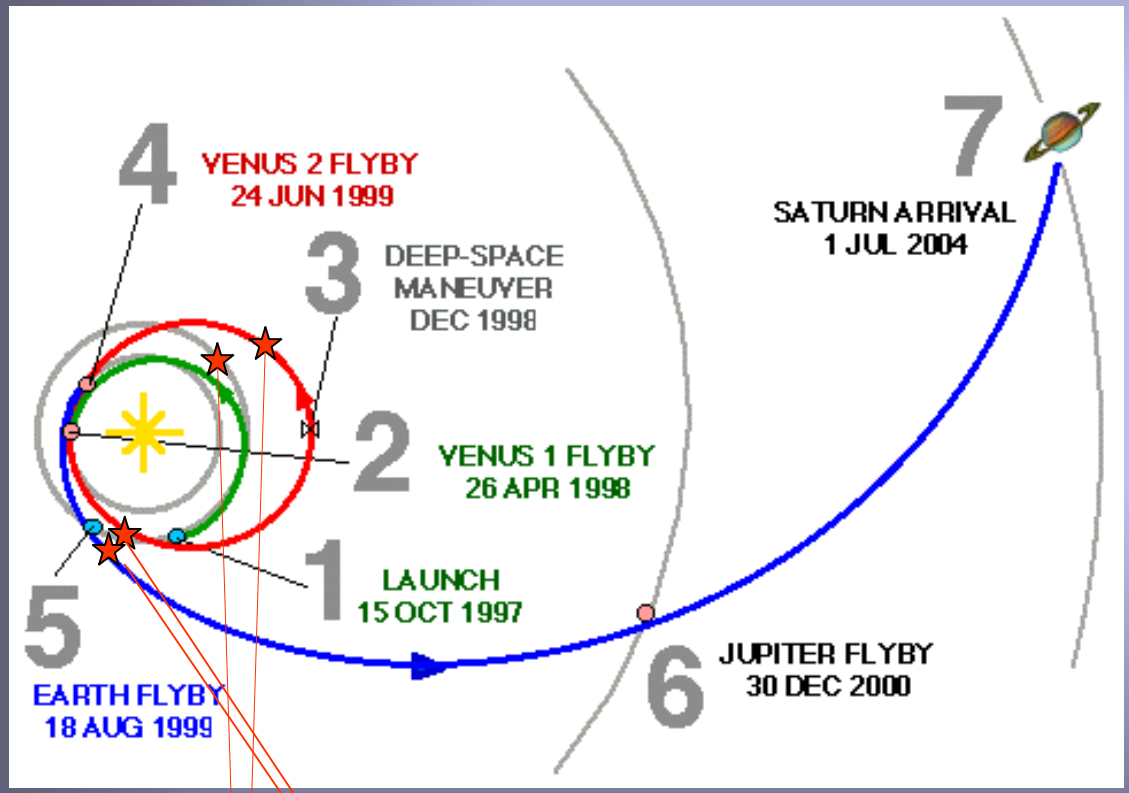

(Kaiser et al., 2000)

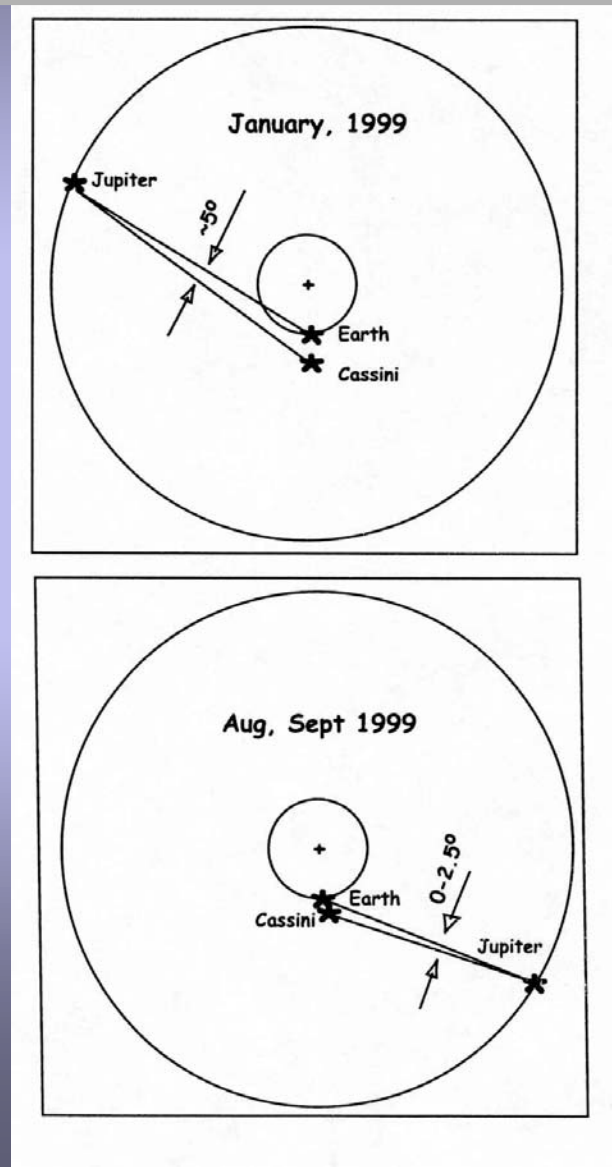

Saturn Orbit Insertion (SOI) July 1, 2004

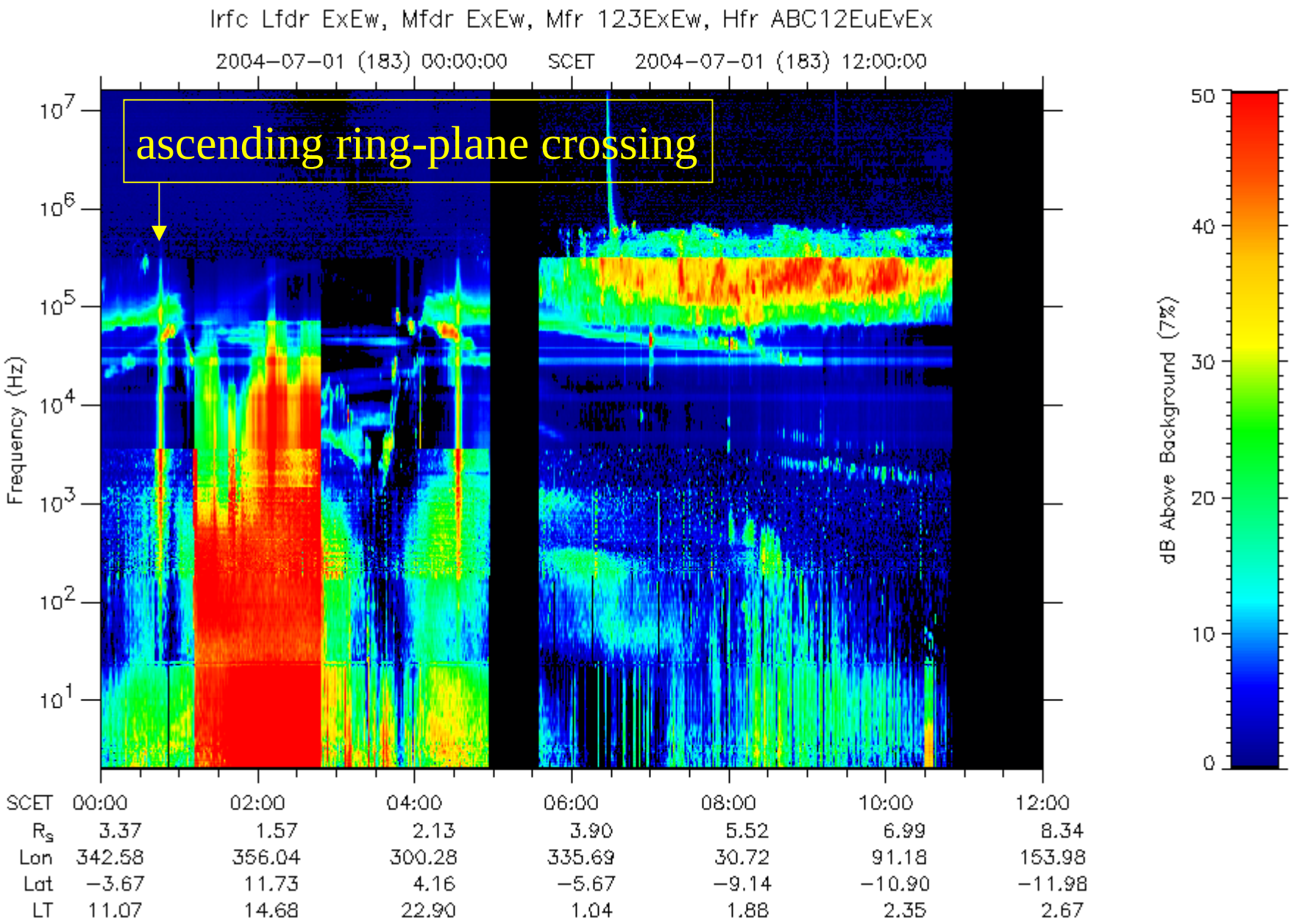

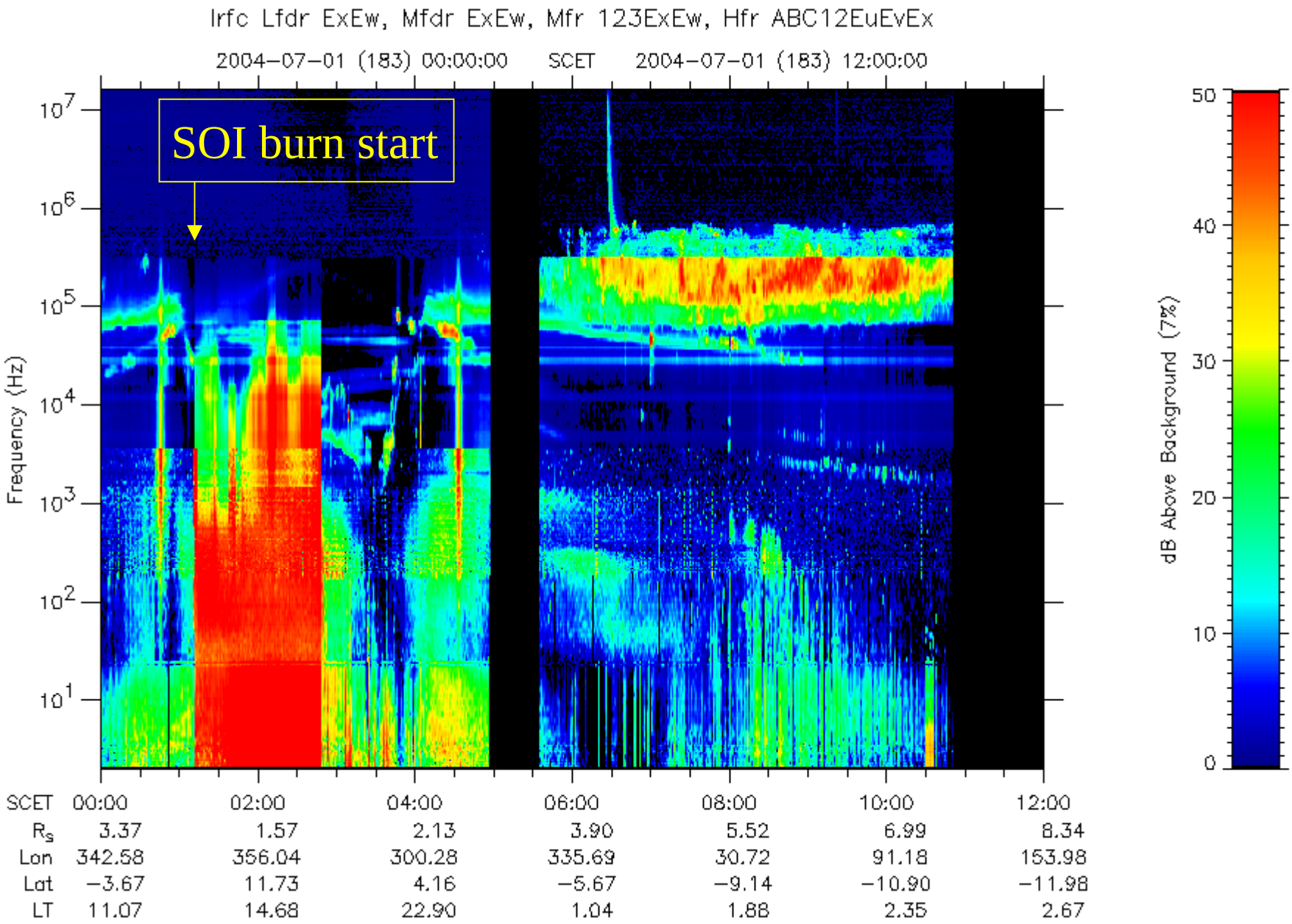
Irfc Lfdr ExEw, Mfdr ExEw, Mfr 123ExEw, Hfr ABC12EuEvEx
2004-07-01 (183) 00:00:00 SCET 2004-07-01 (183) 12:00:00
SOI burn start
Frequency (Hz)
10^7
10^6
10^5
10^4
10^3
10^2
10^1
dB Above Background (7%)
50
40
30
20
10
0
SCET 00:00 02:00 04:00 06:00 08:00 10:00 12:00
R_S 3.37 1.57 2.13 3.90 5.52 6.99 8.34
Lon 342.58 356.04 300.28 335.69 30.72 91.18 153.98
Lat −3.67 11.73 4.16 −5.67 −9.14 −10.90 −11.98
LT 11.07 14.68 22.90 1.04 1.88 2.35 2.67

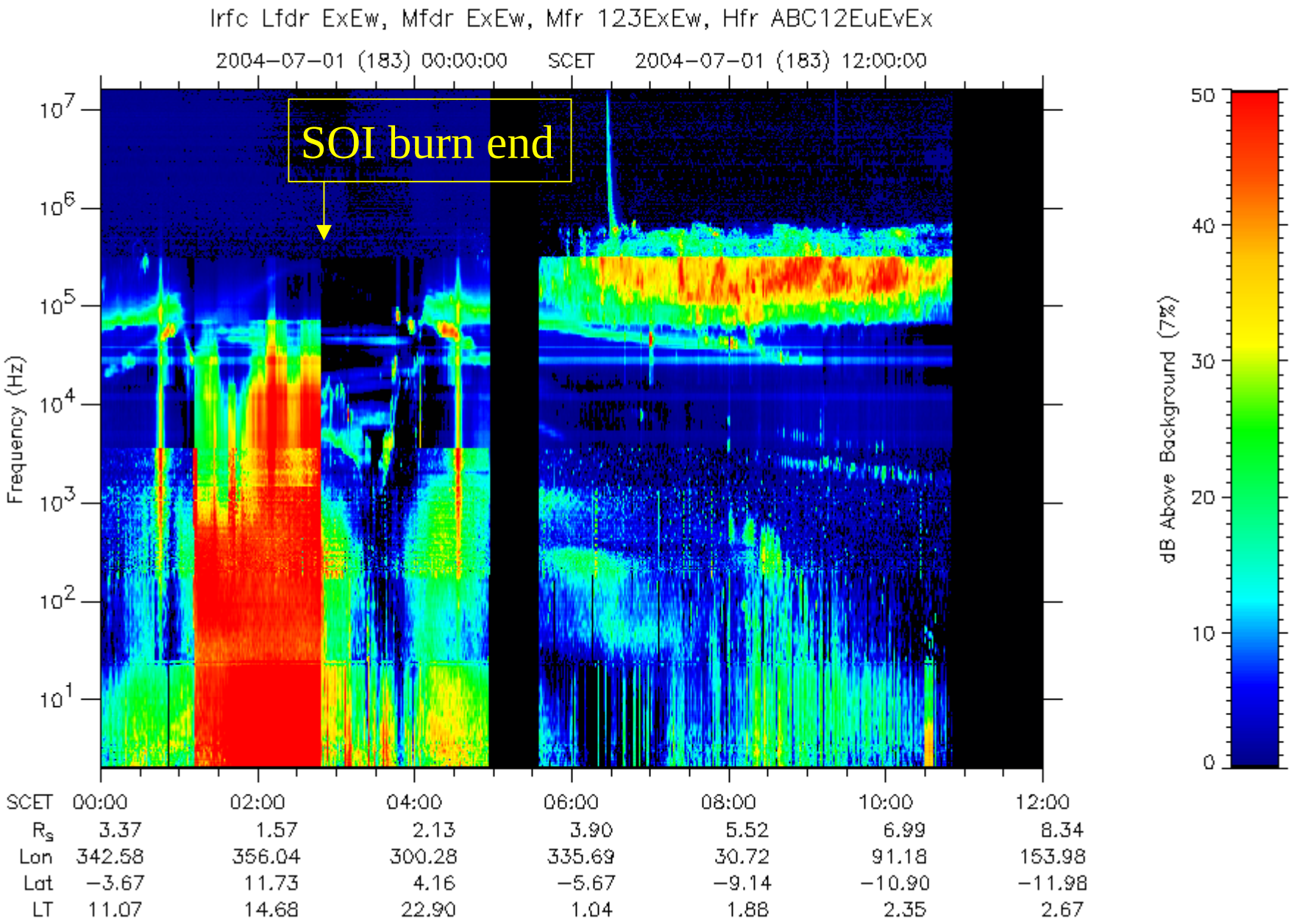
lrfc Lfdr ExEw, Mfdr ExEw, Mfr 123ExEw, Hfr ABC12EuEvEx
2004-07-01 (183) 00:00:00 SCET 2004-07-01 (183) 12:00:00
SOI burn end
Frequency (Hz)
10^7
10^6
10^5
10^4
10^3
10^2
10^1
dB Above Background (7%)
50
40
30
20
10
0
SCET 00:00 02:00 04:00 06:00 08:00 10:00 12:00
R_S 3.37 1.57 2.13 3.90 5.52 6.99 8.34
Lon 342.58 356.04 300.28 335.69 30.72 91.18 153.98
Lat −3.67 11.73 4.16 −5.67 −9.14 −10.90 −11.98
LT 11.07 14.68 22.90 1.04 1.88 2.35 2.67

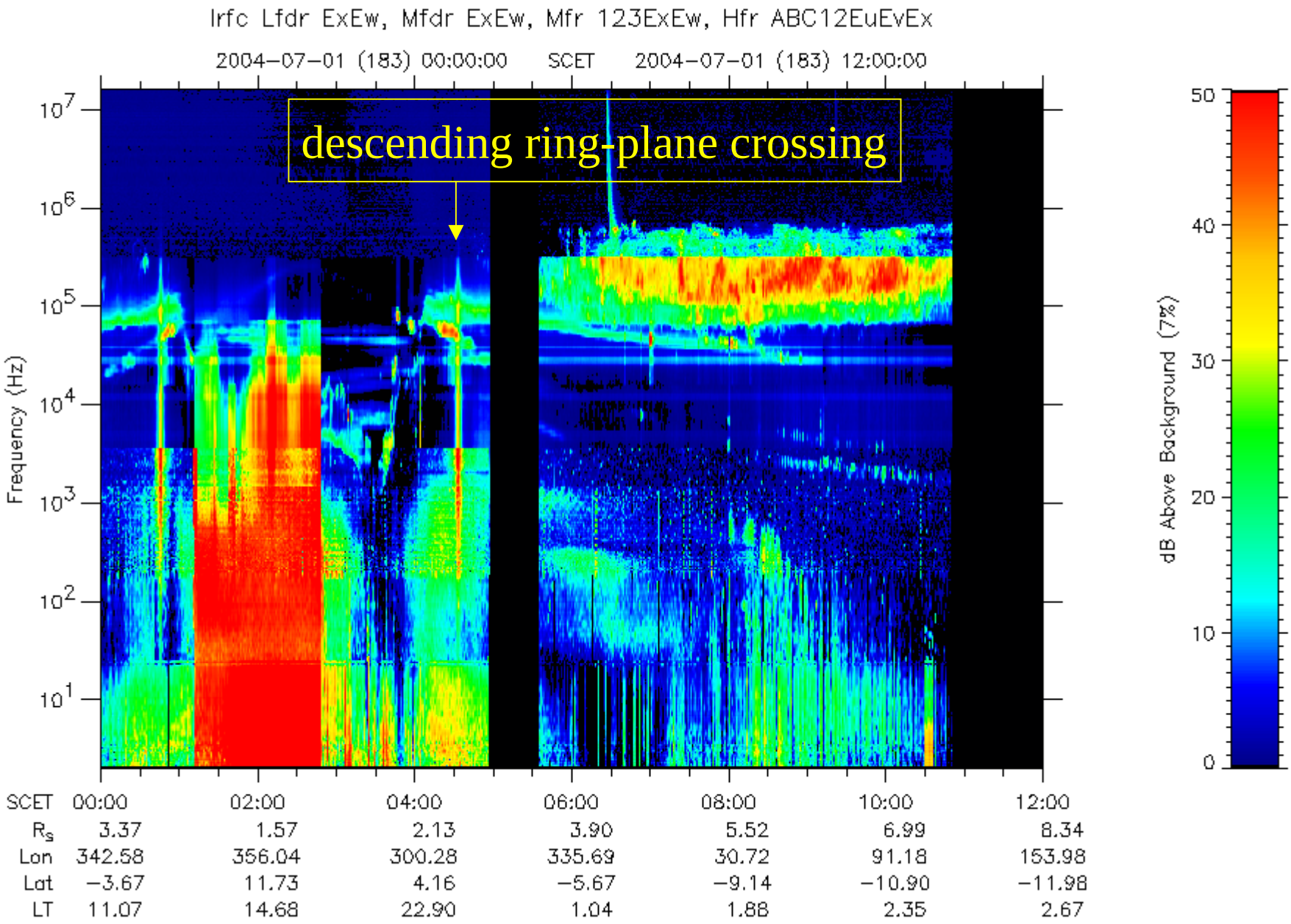
lrfc Lfdr ExEw, Mfdr ExEw, Mfr 123ExEw, Hfr ABC12EuEvEx
2004-07-01 (183) 00:00:00 SCET 2004-07-01 (183) 12:00:00
descending ring-plane crossing
Frequency (Hz)
10^7
10^6
10^5
10^4
10^3
10^2
10^1
dB Above Background (7%)
50
40
30
20
10
0
SCET 00:00 02:00 04:00 06:00 08:00 10:00 12:00
R_S 3.37 1.57 2.13 3.90 5.52 6.99 8.34
Lon 342.58 356.04 300.28 335.69 30.72 91.18 153.98
Lat −3.67 11.73 4.16 −5.67 −9.14 −10.90 −11.98
LT 11.07 14.68 22.90 1.04 1.88 2.35 2.67

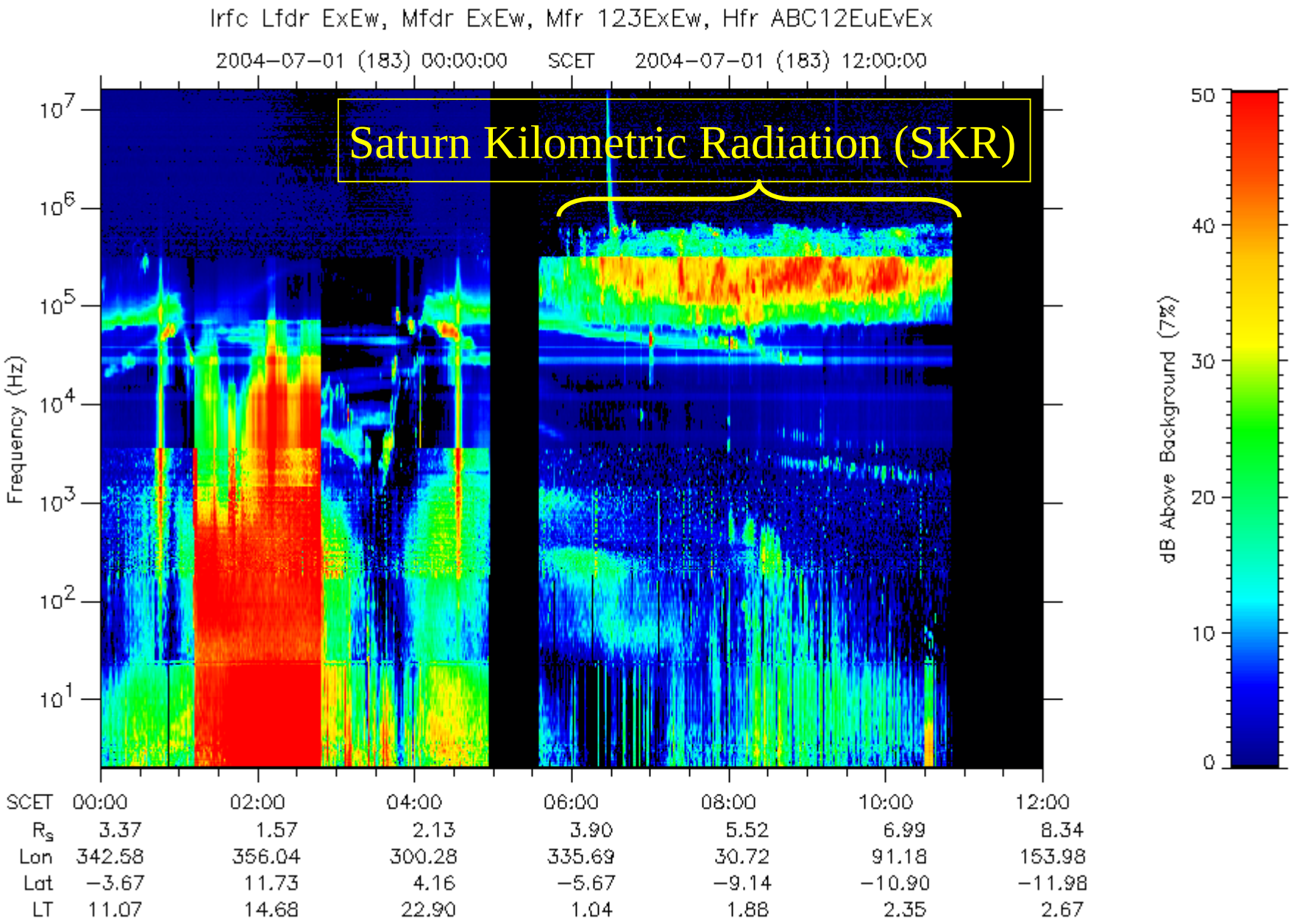
lrfc Lfdr ExEw, Mfdr ExEw, Mfr 123ExEw, Hfr ABC12EuEvEx
2004-07-01 (183) 00:00:00 SCET 2004-07-01 (183) 12:00:00
Saturn Kilometric Radiation (SKR)
Frequency (Hz)
10^7
10^6
10^5
10^4
10^3
10^2
10^1
dB Above Background (7%)
50
40
30
20
10
0
SCET 00:00 02:00 04:00 06:00 08:00 10:00 12:00
R_S 3.37 1.57 2.13 3.90 5.52 6.99 8.34
Lon 342.58 356.04 300.28 335.69 30.72 91.18 153.98
Lat −3.67 11.73 4.16 −5.67 −9.14 −10.90 −11.98
LT 11.07 14.68 22.90 1.04 1.88 2.35 2.67

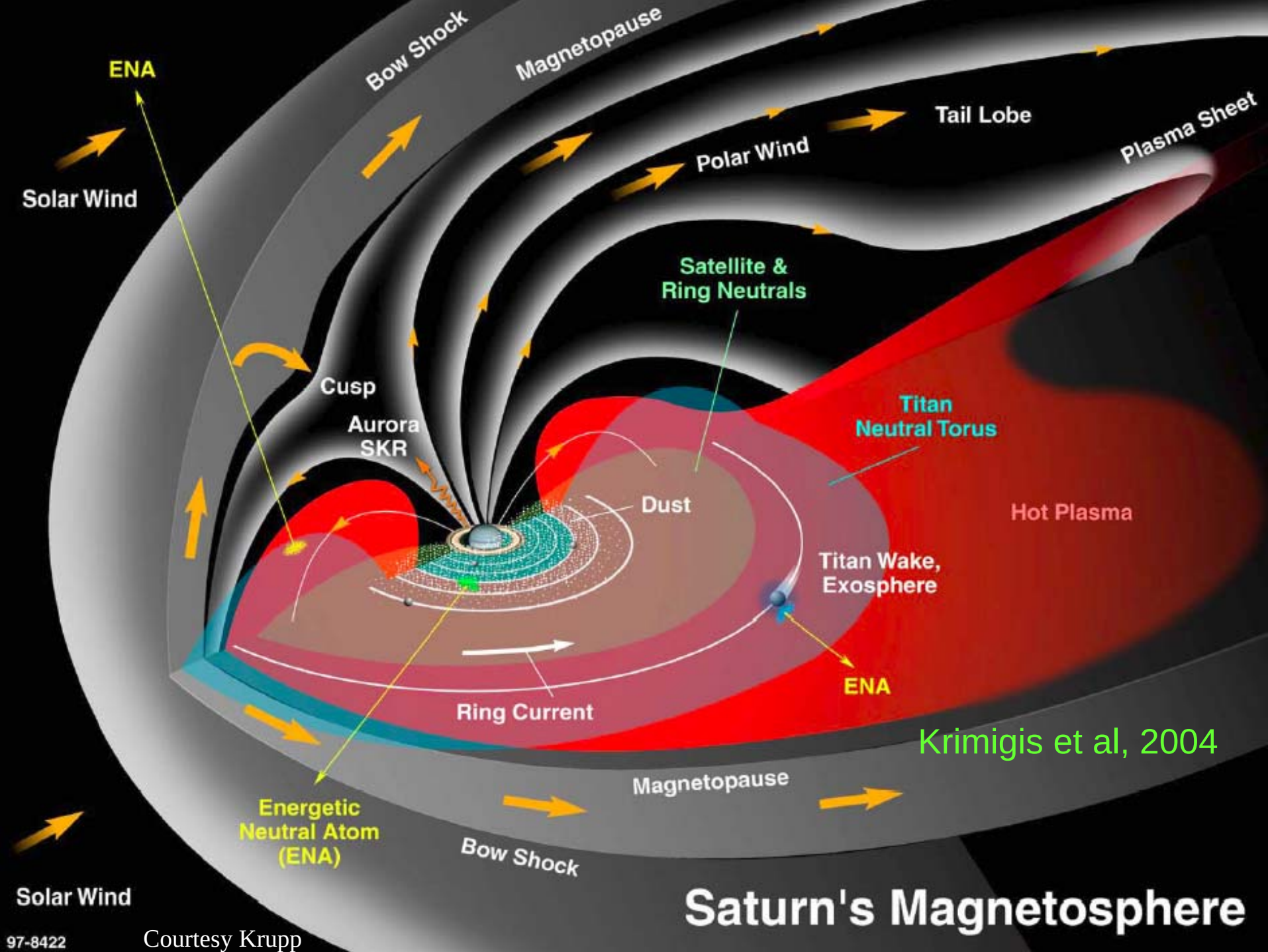
ENA
Bow Shock
Magnetopause
Solar Wind
Polar Wind
Tail Lobe
Plasma Sheet
Satellite &
Ring Neutrals
Cusp
Aurora
SKR
Titan
Neutral Torus
Dust
Hot Plasma
Titan Wake,
Exosphere
ENA
Ring Current
Krimigis et al, 2004
Magnetopause
Energetic
Neutral Atom
(ENA)
Bow Shock
Solar Wind
Saturn's Magnetosphere
97-8422
Courtesy Krupp

Saturn Kilometric Radiation (SKR)

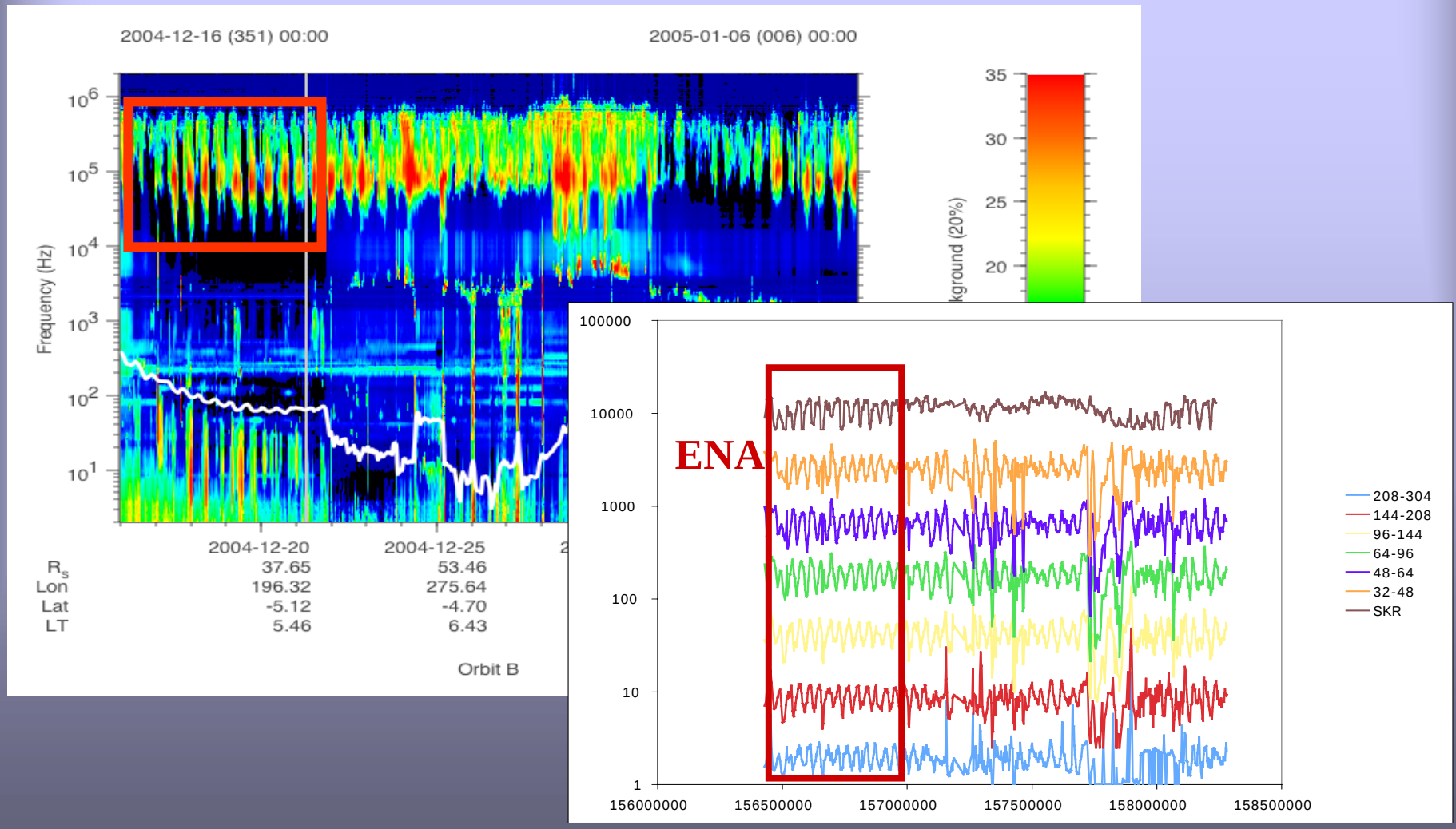

Courtesy Krupp

External control of SKR

Voyager 2 SKR Observations:

$$\frac{E}{\Omega} = S\Delta f\left(\frac{d^2}{\Omega}\right)\Delta t$$

$$P_{ram} = \rho v^2$$

B_{IMF}

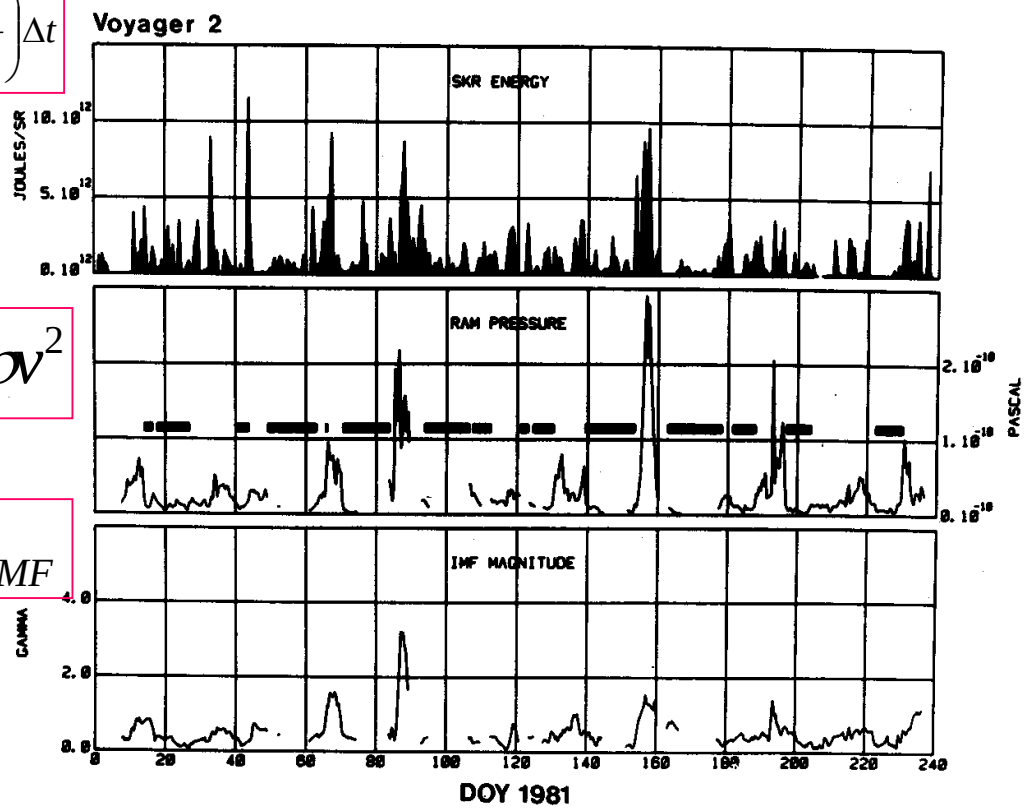

Figure 5

Voyager 2 observations of the Saturn kilometric radiation, the solar wind ram pressure, and the interplanetary magnetic field strength, ballistically propagated from the point of observation (= spacecraft) to the interaction point (position of Saturn). Note the good coincidence of the upper two profiles and the sudden decreases of the parameters during Jovian magnetotail events, indicated by bars in the second panel (DOY*= *day of year*) (*Rucker and Desch*, 1986).

External control of SKR

Voyager 2 approaching Saturn: Indications on distant Jupiter magnetotail

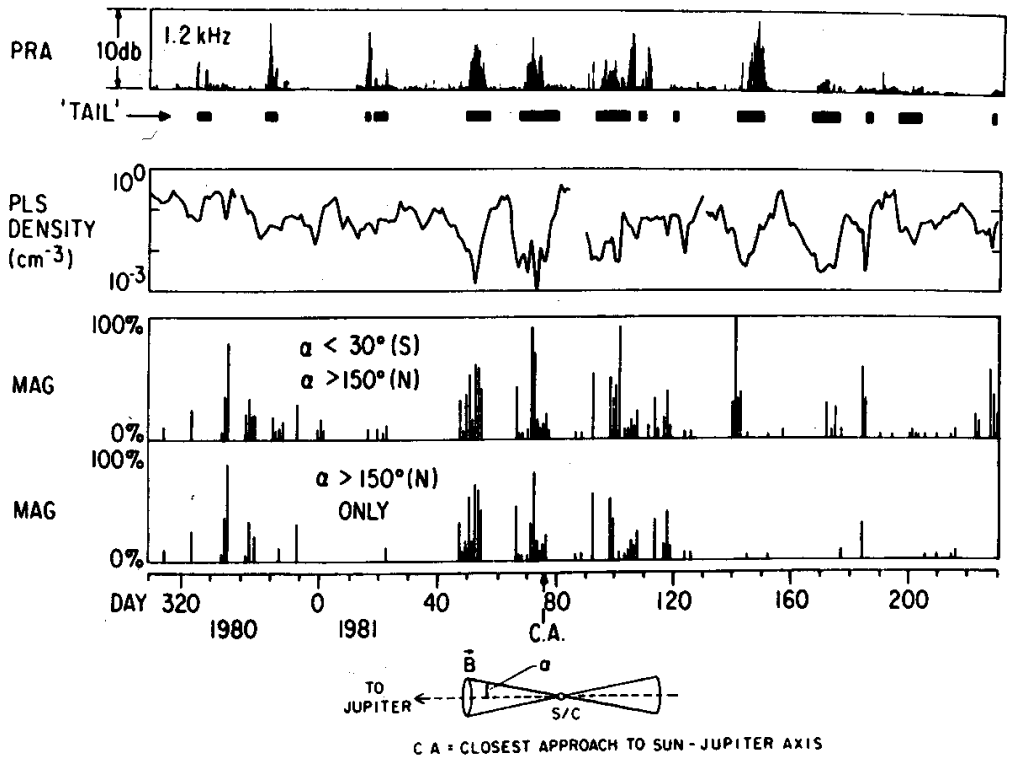

Figure 4

Voyager 2 observations of the distant Jupiter magnetotail as indicated by the bars between the first and second panel. Within the plasma depleted tail filaments, indicated by extreme low plasma densities (second panel), the Jovian continuum radiation, measured by the 1.2 kHz PRA *channel (first panel) is traced along the Jovian magnetotail and detected during tail encounter periods. The lower panels show the tail-like magnetic field orientation, which apparently follows the radial sun-Jupiter line (adapted from Lepping* et al., 1982 ; 1983). (© American Geophysical Union, 1982).

External control of SKR

Voyager 2 SKR observations:

Jupiter magnetotail filaments, propagated to the position of Saturn

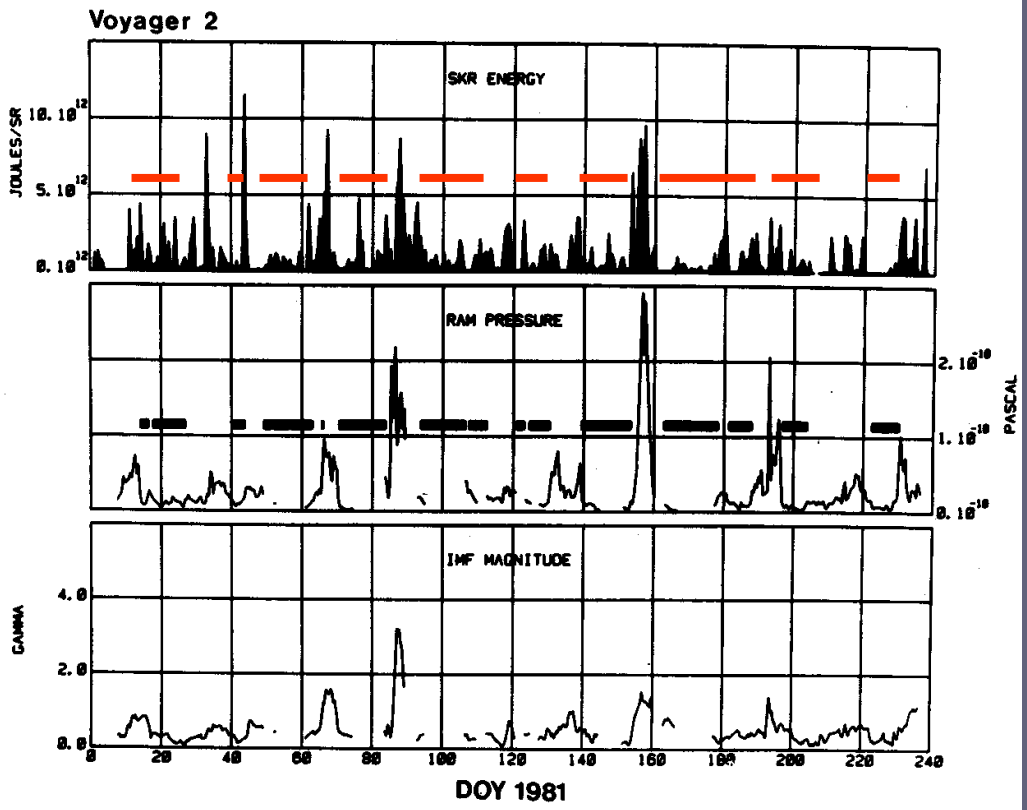

Figure 5

Voyager 2 observations of the Saturn kilometric radiation, the solar wind ram pressure, and the interplanetary magnetic field strength, ballistically propagated from the point of observation (= spacecraft) to the interaction point (position of Saturn). Note the good coincidence of the upper two profiles and the sudden decreases of the parameters during Jovian magnetotail events, indicated by bars in the second panel (DOY* = *day of year*) (*Rucker and Desch*, 1986).

Jupiter ground-based observations

European Decameter Radio Stations

Nancay (~ 0°)

Graz (~ 15° E)

Kharkov (~ 37°)

Jupiter ground-based observations

Table 2
The European decametre radio telescopes network

Radio station	Location coordinates	Operating range (MHz)	Physical aperture (m)	Maximum effective area at 25 MHz (m^2)	Number of array elements	Element antenna	Polarisation	Beam width at 25 MHz	Distance to UTR-2 (km)	Angular resolution at 25 MHz
UTR-2 N–S	Kharkov, Ukraine	8–32	1800 × 60	100000	1440	Dipole	1 linear	0.3° × 12°	0	0.4° × 0.4°
UTR-2 E–W	49°N, 37°E	8–32	900 × 60	50000	600	Dipole	1 linear	0.6° × 12°	0	
URAN-1	Zmiev, Ukraine 49°N, 36°E	8–32	240 × 28	5500	95	Crossed dipoles	2 linear	24° × 3°	42	60″
URAN-2	Poltava, Ukraine 49°N, 34°E	8–32	240 × 112	28000	512	Crossed dipoles	2 linear	6° × 3°	120	21″
URAN-3	Lviv, Ukraine 51°N, 24°E	8–32	240 × 56	14000	256	Crossed dipoles	2 linear	12° × 3°	915	2.7″
URAN-4	Odessa, Ukraine 46°N, 30°E	8–32	240 × 28	7300	128	Crossed dipoles	2 linear	24° × 3°	613	4.0″
Nançay Decametre Array	Nançay, France 47°N, 2°E	8–88	100 × 100	2 × 4000	2 × 72	Conical Helix spiral	2 circular	6° × 12°	3000	n.a.
Lustbühel	Graz, Austria 47°N, 15°E	13–32	n.a.	2 × 300	2	Log-periodic linear	2 linear	60° × 60°	1800	n.a.

Lecacheux et al., Using large radio telescopes at decametre wavelengths, PSS Special Issue on LOFAR and (Extra-)Solar System Science, 52, 1357, 2004.

Jupiter ground-based observations

INTAS C2 Kampagne 2000

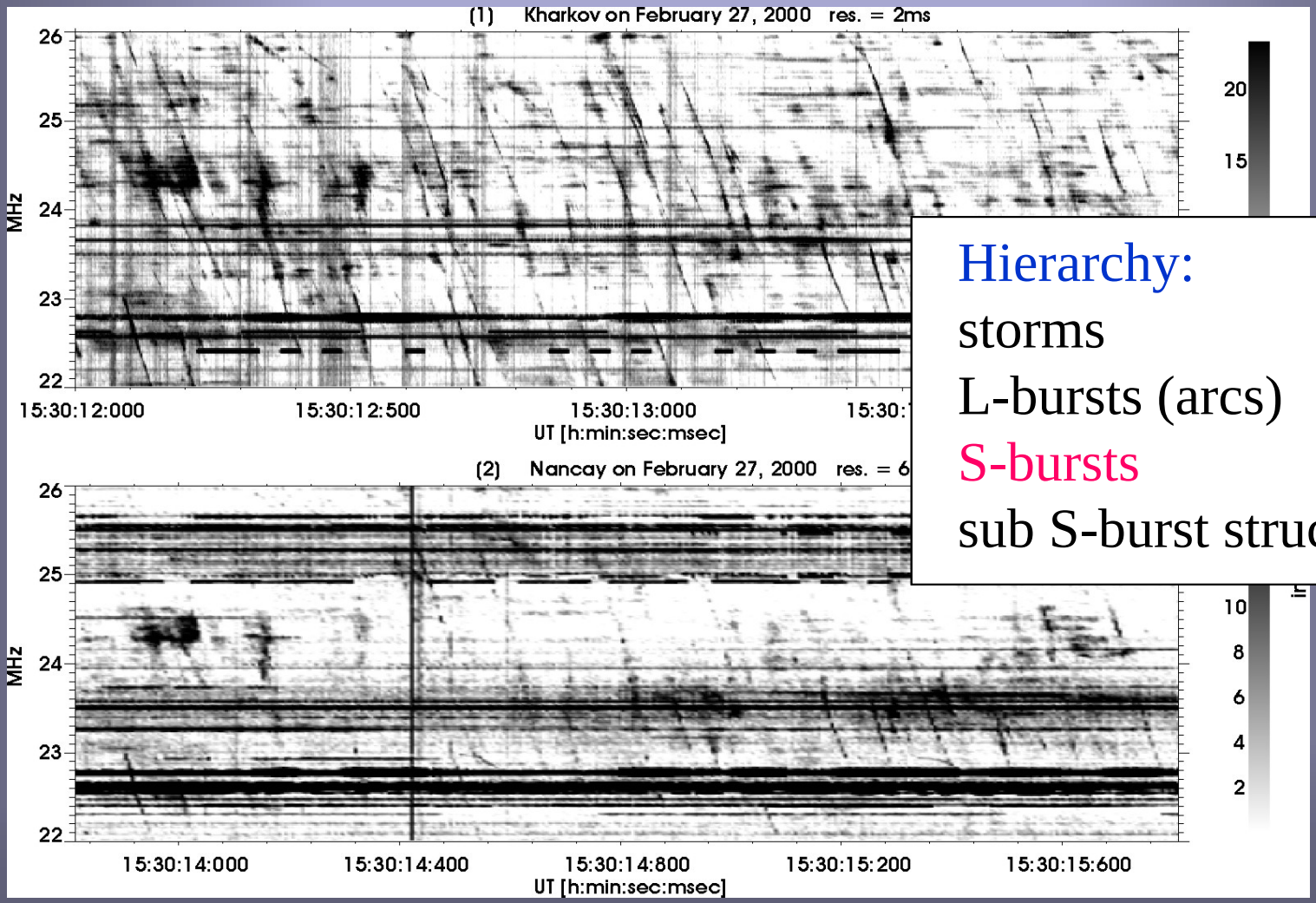

Hierarchy:

storms

L-bursts (arcs)

S-bursts

sub S-burst structures

Jupiter ground-based observations

INTAS C2 Kampagne 2000

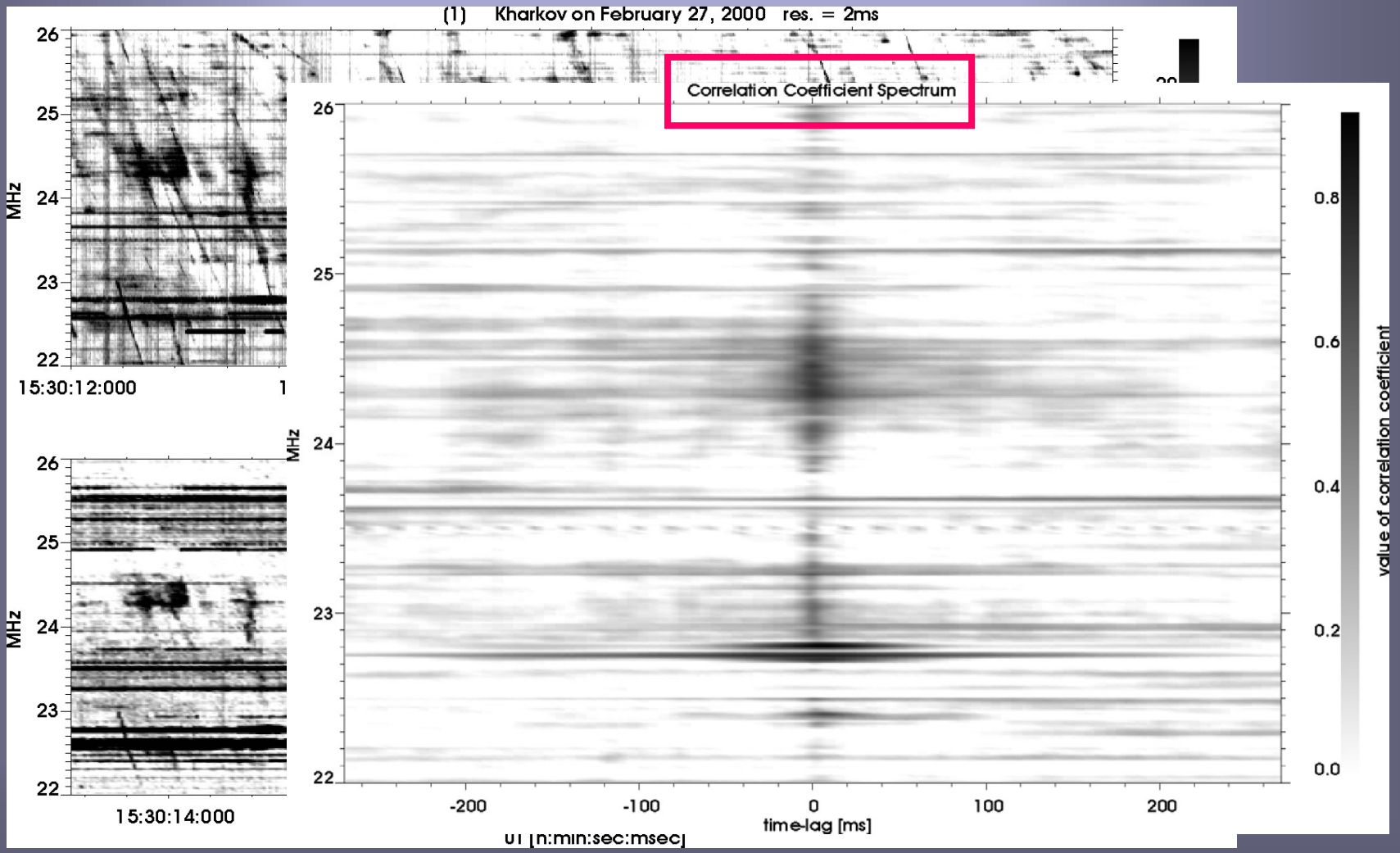

Jupiter ground-based observations

Hierarchy:
storms
L-bursts (arcs)
S-bursts
sub S-burst structures

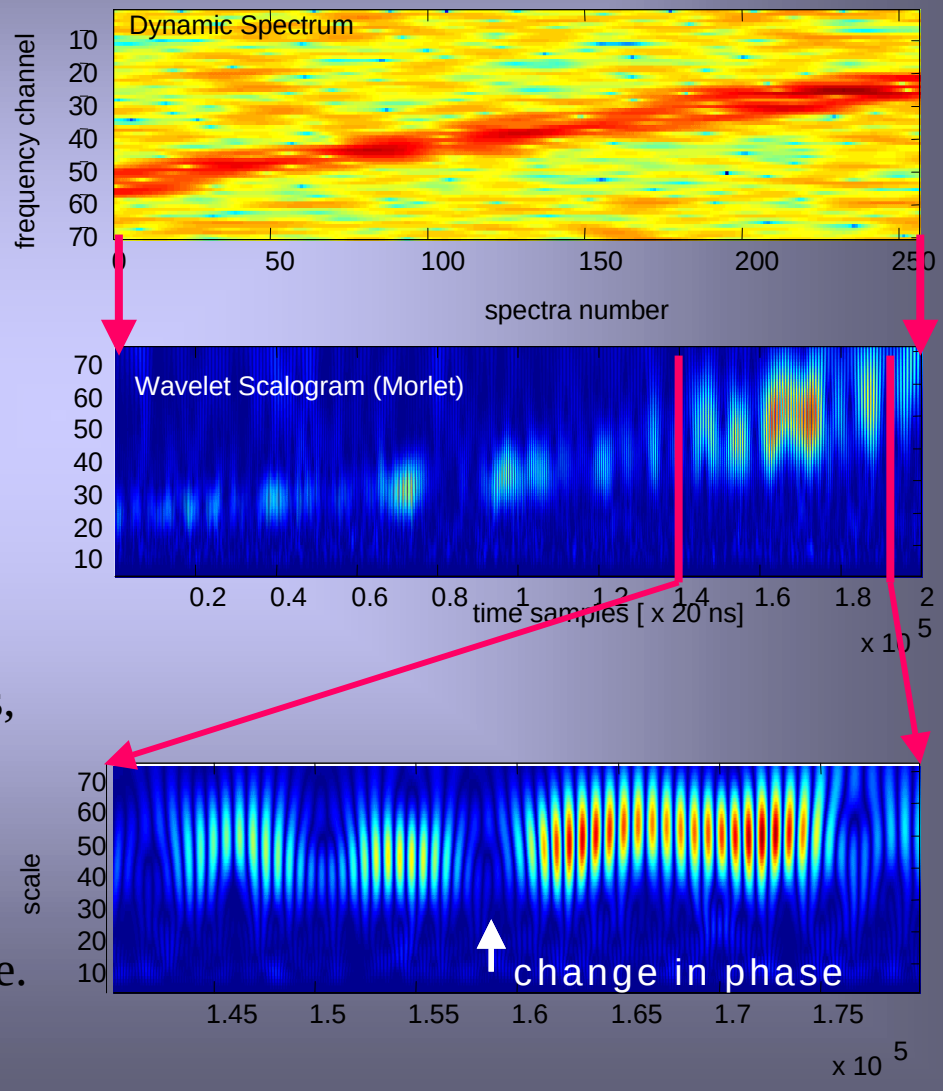

Carr, T.D. and F. Reyes, Microstructure of Jovian Decametric S-bursts, JGR, 1999.

Leitner, M., Waveform analysis techniques of Jovian S-bursts observations, PhD Thesis, Univ. Graz, 2001.

Litvinenko, G., H.O. Rucker, et al., Internal structure of the Jovian simple S-burst obtained with the wavelet analysis technique. Astron.Astrophys., 426, 343, 2004.